2023

Split Catalytic Probes for the Detection of Monkeypox Virus

Jaehyun Ahn
University of Central Florida

SPLIT CATALYTIC PROBES FOR THE DETECTION OF MONKEYPOX VIRUS

by

JAEHYUN AHN

A thesis submitted in partial fulfillment of the requirements
for the Interdisciplinary Thesis in Chemistry
in the College of Sciences
and in the Burnett Honors College
at the University of Central Florida
Orlando, Florida

Summer Term, 2023

Thesis Chair: Yulia Gerasimova, Ph.D.

ABSTRACT

The COVID-19 outbreak highlighted the important role that diagnostic tests play in the healthcare system. To reduce the impact of infectious disease outbreaks, the development of rapid and cost-effective point-of-care-tests (POCTs) is crucial. With the dissemination of the Monkeypox (Mpox) virus, it became a necessity to produce POCTS that are inexpensive and easy to use. This work explored the construction of two colorimetric assays that aim to detect Mpox genetic signatures. One is based on the split-peroxidase-like deoxyribozyme probes (sPDz), while the other utilizes a cascade system of split RNA-cleaving deoxyribozyme (sDz) and peroxidase-like deoxyribozyme (PDz). Both rely on catalytic probes as well as a G-Quadruplex (G4) structure to facilitate the production of a color change in the presence of the genetic signatures of Mpox. The sPDz probes were initially tested with synthetic genomic fragments of Mpox and other Orthopoxviruses for selectivity purposes. The sPDz probes were then further optimized. The optimal sPDz probes and the sDz/PDz cascade system were tested with an amplified genome fragment of Mpox. The genome fragments were generated by using both symmetric and asymmetric polymerase chain reaction (PCR). With further optimization to increase the signal-to-background ratio, these probes may show promise as an assay that may have the potential to be incorporated to develop POCTs.

ACKNOWLEDGEMENT

I would like to first thank Dr. Yulia Gerasimova for providing me with the opportunity to perform research and explore areas in biochemistry that I never knew of. Her patience, wisdom and guidance made this thesis possible.

In addition, I would like to specially thank Dr. Ryan Connelly for his knowledge and mentorship during my early stage in the lab.

I am grateful to my committee members for taking their support throughout my thesis.

I would like to thank the College of Science for awarding me the 2023 Honors Undergraduate Thesis Scholarship, as well as the Office of Undergraduate Research for their Fall 2022 Student Research Grant.

Finally, I would like to thank all my friends and family members for encouraging me to do my best.

This work was also possible due to the resources provided by BEI resources. "The following reagents were obtained through BEI Resources, NIAID, NIH: Genomic DNA from Monkeypox Virus, hMPXV/USA/MA001?2022 (Lineage B.1, Clade IIb), NR-58710, Genomic DNA from Cowpox Virus, Brighton Red, NR-2641, and Genomic DNA from Vaccinia Virus, IHD, NR-2636."

TABLE OF CONTENTS

LIST OF FIGURES

LIST OF TABLES

LIST OF ABBREVIATIONS

ABTS	2,2’-azino-bis (3-ethylbenzothiazoline-6-sulfonic acid)
AS	Associated State
CDC	Centers for Disease Control
CPOX_T60	Cowpox Synthetic Target
C3L	Complement binding protein 3
DS	Dissociated State
DAB	3,3’-diaminobenzidine
dsDNA	Double stranded DNA
FP	Forward Primer
FRET	Fluorescence Resonance Energy Transfer
G4	G-Quadruplex
IPDz	Inhibited peroxidase-like deoxyribozyme
LATE-PCR	Linear-After-The-Exponential Polymerase Chain Reaction
MP_T60	Mpox Synthetic Target
MSM	Men who have sex with men
Mpox	Monkeypox
NTC-2A	No-Target-Control with Primer Set FP and LATE-RP-2

NTC-S	No-Target-Control with Primer Set FP and RP-A
PDz	Peroxidase-like deoxyribozyme
POCT	Point-of-care Tests
qPCR	Real time PCR
RP	Reverse Primer
ssDNA	Single stranded DNA
sDz	Split RNA-cleaving deoxyribozyme
sPDz	Split Peroxidase-like deoxyribozyme
SNP	Single Nucleotide Polymorphisms
Tm	Melting Temperature
TNF	Tumor Necrosis Factor
VARV	Variola Virus
VACV	Vaccinia Virus
WHO	World Health Organization

INTRODUCTION

Background Information

On July 23, 2022, Dr. Tedros Adhanom Ghebreyesus, the Director-General of World Health Organization (WHO), classified the Monkeypox (Mpox) virus as a Public Health Emergency of International Concern.[1] Such declaration accentuated the magnitude of danger that Mpox posed to the global community. Mpox was first discovered in Denmark among cynomolgus monkeys in 1958.[2] For human infection, the first case occurred in a child from the Democratic Republic of Congo in 1970.[3] Prior to the breakout in 2022, Mpox was endemic in west and central African nations.[3,4] However, in May of 2022, reports of Mpox infections outside the endemic region began to arise.[4] As this event followed the COVID-19 pandemic, the advent of Mpox posed as a potential threat for another global health crisis.

Although Mpox is a zoonotic virus, analysis of the current outbreak in non-endemic regions indicated a low possibility for animal-to-human transmission to be the main source of the outbreak.[5] This is because the natural animal reservoir has yet to be determined for the outbreaks in non-endemic regions.[5] Mpox virus can disseminate through contact with one of the following: bodily fluids, lesions, and respiratory droplets.[4] Data compiled by WHO shows that the spread of Mpox has been more widely prevalent in men who have sex with men (MSM).[4] As of July 19th, 2023 at 2 PM EDT, there have been 88,549 cases world-wide, with 30,611 of those from the United States.[6] To prevent further growth in number of cases, it is imperative to develop an efficient POCT to address this outbreak as rapid, accurate diagnostic tests are essential for surveillance and disease-prevention.

The current gold-standard diagnostic assay for Mpox is real-time Polymerase-Chain reaction (qPCR).[7] Therefore, it is the current standard protocol used for Mpox diagnostics. However, to utilize qPCR, expensive thermocyclers and trained laboratory technicians are required.[7] Such quality makes qPCR an unfavorable choice for a POCT. Based on the criteria suggested by Drain et al, POCT should be rapid, have an acceptable test-efficacy and be cost-effective.[8] A POCT based on a colorimetric assay that utilizes a split catalytic probe based on deoxyribozymes may be a valuable alternative as it uses color change for detection, which can be read by the naked eye.[9]

Monkeypox Virus's Characteristics and Properties

Monkeypox virus is a linear, double-stranded DNA (dsDNA) virus that is part of the *Orthopoxvirus* genus and *Poxviridae* family.[2] The *Orthopoxvirus* genus includes well known viral pathogens such as vaccinia virus (VACV) and variola virus (VARV).[2] The latter is known to cause smallpox.[2] Based on genomic analysis, two distinct clades of the Mpox were identified: Clade I (formerly known as Congo Basin/Central African) and Clade II (formerly known as West African).[10] The latter is comprised of two separate subclades, Clade IIa and Clade IIb.[10] Each clade has different characteristics regarding fatality. Clade I have a higher fatality rate (up to approximately 11-12%) than Clade II.[2,11]

As Mpox and VARV are in the same genus and family, they have similar clinical characteristics. They both have an incubation phase that lasts across multiple days.[2,11-13] For the current Mpox 2022 outbreak, the incubation period can vary from 7 to 10 days, depending on the population case studied.[11] For smallpox, the incubation period is known to vary from 7 to 17 days.[12,13] These pathogens induce an initial prodromal period that includes symptoms such as

fever and headache. [2,11-13] In addition, both pathogens cause rashes to form. [2,11-13] For both Mpox and VARV, the spread of the lesion and rashes can be described as a centrifugal distribution.[13,14] The rash produced in the Mpox occurs in four stages: (1) macular, (2) papular, (3) vesicular, (4) pustular.[2,13] Although the Mpox has common clinical characteristics with VARV, the identification of lymphadenopathy is unique to the former; therefore, it is a distinguishing factor between the two.[2,13]

Although the average fatality rate of the Mpox isn't as high as that of VARV, that should not be a reason to ignore the disease as it has other negative outcomes. According to a clinical study conducted by WHO in 1987 in Zaire (now known as Democratic People's Republic of Congo), the death rate among children between 0 to 4 was 14.9% and between 5 to 9 was 6.5%.[14] Pregnant women are also vulnerable to complications. Although further extensive studies must be done, there have been cases in which Mpox has impacted the health of the mother and the baby.[11,15] From 2007 to 2011, 4 cases of pregnant women with Mpox were studied.[11,15] Out of these four women, two experienced miscarriage, and one had a fetal death.[11,15] These cases emphasize the necessity to develop a reliable yet rapid approach to diagnose and/or prevent further transmission of Mpox virus to protect those that are most vulnerable.

Current Possible Diagnostic Methods.

With the advent of Mpox, numerous diagnostic methods were developed.[16] These methods include diagnostics based on culture, immunodiagnostics, isothermal amplification methods, and PCR.[16] Virus detection based on conventional cell culture is not feasible for a rapid diagnostic test as it can take multiple days for the virus to grow.[17] In addition, virus cultures require facilities with high biosafety levels and complex laboratory equipment as well as highly trained technician that can interpret the data.[16] Usage of antibody detection for Mpox diagnostics is not suggested by the WHO as it may not differentiate among Orthopoxviruses.[18]

Background of Real Time Polymerase Chain Reaction

The current gold standard for Mpox detection is qPCR as it is sensitive and specific.[7] Therefore, it is the method that is currently recommended by WHO for the purpose of Mpox diagnostics.[18] qPCR includes similar steps of just regular PCR – denaturation, annealing, and extension – but incorporates generation of a fluorescent signal as the target gets amplified. Unlike the standard PCR, qPCR does not require gel analysis and allows visualization of data in real-time.[19,20] The mechanism behind the visualization is based on the usage of a fluorescent dye (e.g., SYBR Green), hydrolysis probes (e.g., TaqMan Probes), or molecular beacons as shown in Figure 1.[19-22] The first method is based on dyes that are attracted toward the dsDNA and intercalate themselves with the DNA (Figure 1A).[19-21] As the number of dsDNA copies created by the qPCR increases exponentially, the magnitude of the brightness of the fluorescence will be strongly enhanced.[19-21] The second method utilizes hydrolysis probes that are complementary to the specific gene of interest rather than depending on target nonspecific dyes (Figure 1B).[19-21] Each probe is comprised of a fluorescent reporter molecule on the 5'-end and a quencher on the

3’-end.[19-21] As the fluorescent molecule and the quencher are in near proximity, the quencher will inhibit the fluorescence of the reporter molecule.[19-21] Such phenomenon is based on the Fluorescence Resonance Energy Transfer (FRET) mechanism.[19,20] In the presence of the target sequence, the probes will bind and anneal to the target of interest.[19-21] As the extension stage progresses, the *Taq* DNA polymerase will cleave the probe from the 5’-end and separate the quencher from the reporter molecule (Figure 1B).[19-21] Consequently, the fluorescence will be restored and allow the signal reading to occur.[19-21] With every cycle, as more copies of the amplified gene fragment are produced, more probes will be cleaved, further strengthening the fluorescence.[19-21] The third method is based on molecular beacons, which is a probe that also contains a fluorophore on the 5’ end and a quencher on the 3’ end (Figure 1C).[22,23] Molecular beacons contains a hairpin structure that allows the quencher to be near the fluorophore in the absence of the fully matched target, which prevents fluorescence.[22] In the presence of the target, the molecular beacon will hybridize to the target and produce fluorescence (step 2 of Figure 1C).[22,23] Unlike the hydrolysis probes, molecular beacon probes are not hydrolyzed nor depends on the hydrolysis for fluorescence.[22,23] Rather, during the extension (step 3 of Figure 1C), the molecular beacon probes are removed instead of being cleaved. [22,23]

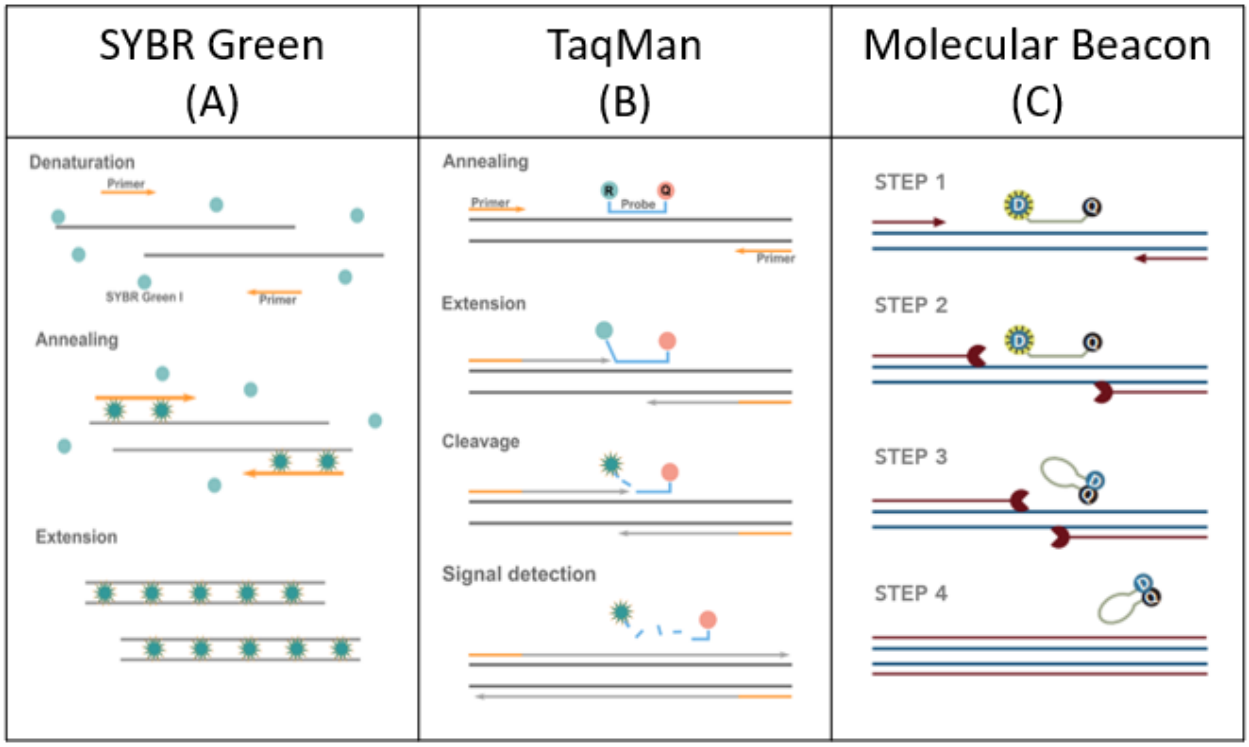

Figure 1: Mechanisms of the fluorescent signal generation in qPCR using (A) dye-based detection (SYBR Green), and (B) hydrolysis probe-based detection (TaqMan) (C) molecular beacon probes-based detection. Reprinted with permission from ref 21 (for A and B)[21]. Copyright 2022. INTEGRA Biosciences. Reprinted with permission from ref 22 (for C).[22] Integrated DNA Technologies.

When compared to each other, there are both advantages and disadvantages of using dyes or probe-based (either TaqMan/hydrolysis or molecular beacon) for qPCR. When using probes, specificity is usually ensured.[20-23] In contrast, dyes are non-specific, and specificity must be determined by analyzing the melting temperature of the amplicons produced.[19] Probes, however, are more expensive than dyes.[20,21,23] In addition, their specificity can be considered as a double-edged sword as each probes cannot be used other than for experiments with the specific target of interest.[20] Dyes, however, can be used for multiple experiments with different targets as it is not sequence specific.[20]

Utilizing qPCR for Mpox Detection

The current qPCR protocol provided by the Centers for Disease Control (CDC) was based on the findings by Li et al. in 2010.[24,25] In this paper, three different assay designs are proposed, G2R_WA (West Africa Specific), C3L (Congo Basin), and G2R_G (Monkeypox virus generic).[24] To design primers and probes (such as TaqMan probes) for the generic assay, the region of the Tumor necrosis factor (TNF) receptor gene was used.[24] That is because the TNF receptor gene contained multiple single nucleotide polymorphisms (SNPs) as well as insertions and deletions among Orthopoxviruses.[24] In addition, the TNF receptor gene was used to design the G2R_WA assay, while a complement binding protein gene (C3L) region was selected to design C3L assay.[24] The C3L gene was selected as known Clade II strains delete this gene and is therefore unique to Clade I.[24] These new assays were able to exhibit selectivity and accuracy necessary for the detection of Mpox genetic signatures.[24]

Introduction to Hybridization and Binary Probes

Hybridization probes are strands, which are usually 15 nucleotides or longer, that bind to its complementary sequence.[26] However, due to the length of the hybridization probes, they are selective in a narrow temperature range.[26,27] Therefore, a melting analysis may be necessary to determine specificity. This problem arises from the fact that a single nucleotide mispairing is not enough to thermodynamically destabilize the mismatched complex.[26] Therefore, an alternative approach in designing the probes was sought. Figure 2 shows free energy diagram that compares the free energy of dissociated state (DS) and either fully matched or mismatched associated states (AS), for nucleic-acid probes of different designs.[26]

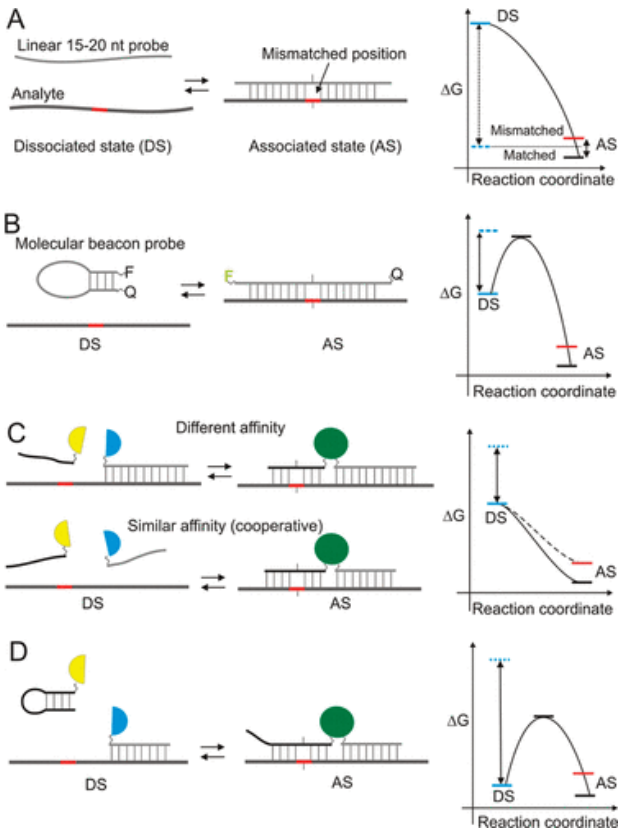

Figure 2: Energy diagrams for the probe-target complex formation predicted for different probe designs.[26] The blue line represents the DS; the black line represents AS with matched target; and the red line represents AS with a mismatched target. (A) Hybridization of a Linear oligonucleotide probe. (B) Hybridization of a molecular beacon probe. (C) Hybridization of binary probes (D) Hybridization with structurally constrained binary probe. Reprinted with permission from ref 26. Copyright 2010 American Chemical Society

As shown in Figure 2A, the energetic penalty of the mismatched AS formation is not costly enough to prevent hybridization when compared to the matched AS duplex.[26] This favors nonselective binding as hybridization will stabilize the system, favoring the AS state in equilibrium, even if it contains a mispairing base. To ameliorate such a problem, the DS state must be lowered in energy to be preferably positioned between the energy states of mismatched and matched AS.[26] To lower the free energy of the DS state, three different methods can be sought. First, a molecular beacon can be used (Figure 2B).[26] Molecular beacons include a hairpin structure, which helps to lower the free energy of the DS state.[26] The magnitude in free energy reduction depends on the length of the stem; however, if the stem is too long, the activation energy can be increased, hindering hybridization.[26] An alternative approach to lower the free energy of the DS state is by using *binary (or split) probes*, in which two different fragments of DNA or RNA are designed to hybridize to the target, as shown in Figure 2C and 2D.[26] The binary probe's design to produce a strong signal (e.g., fluorescence) only when the two parts hybridizes to the analyte in proximity provide a great discriminating power.[26] In addition, one of the probes can be designed to constrain the target-binding arm (Figure 2D), which can facilitate the reduction of the free energy of the DS state even further and position it between the energy state of the matched and mismatched AS states.[26] Therefore, different designs of binary probes will be explored for the purpose of designing a sensor with the potential for high selectivity.

Split Peroxidase Like Deoxyribozymes Probes

Split peroxidase like deoxyribozyme probes (sPDz) is a type of binary probe that depends on a G-Quadruplex (G4) structure as its functional unit for signal production[9,26,28]. G4 is a secondary structure formed by the stacking of G-quartet which is formed from the interaction of four guanines through Hoogsteen base pairing (Figure 3A).[29,30] G4's structure includes loops (Figure 3B) and flanks.[30] The flanking sequences are nucleotide sequences that precede the first sets of guanine triplets in the 5' end or sequences that follows the last sets of guanine triplets in the 3' end. It is known that monovalent ions such as K^+ and Na^+ can promote the formation of G4 by stabilizing the structure.[29]

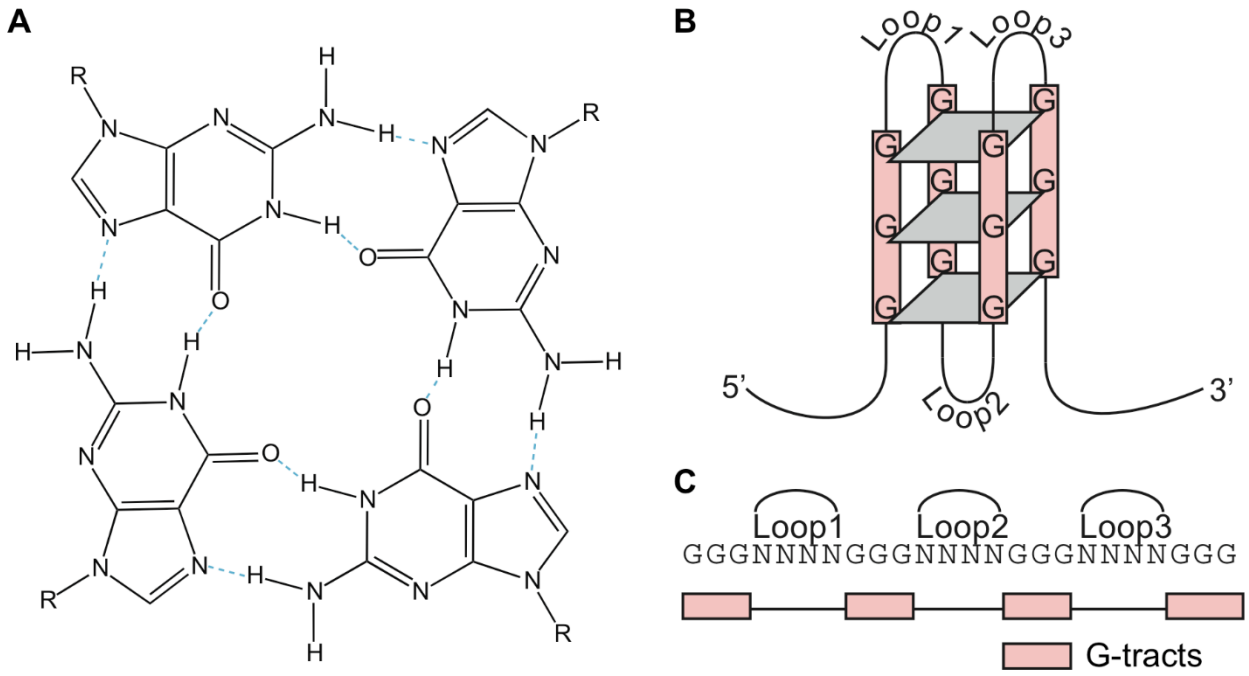

Figure 3: (A) Structure of a G-Quartet.[30] Each adjacent guanines hydrogen bonds to each other. (B) A unimolecular G4 structure.[30] Each loop represents nucleotide sequences between two triplets of guanines. Reprinted with permission from ref 30. Copyright 2010 Public Library of Science.

In the presence of hemin [iron (III)-protoporphyrin IX], G4 is known to behave like a "peroxidase".[26,29] This hemin-G4 complex can be then used to catalyze the oxidation of a colorless substrate such as 2,2'-azino-bis (3-ethylbenzothiazoline-6-sulfonic acid) (ABTS) to produce a colored oxidized product that can be seen with the naked eye.[9] The proposed mechanism of G4 with $ABTS^{2-}$ in the presence of hemin and H_2O_2 is shown in Figure 4.[31]

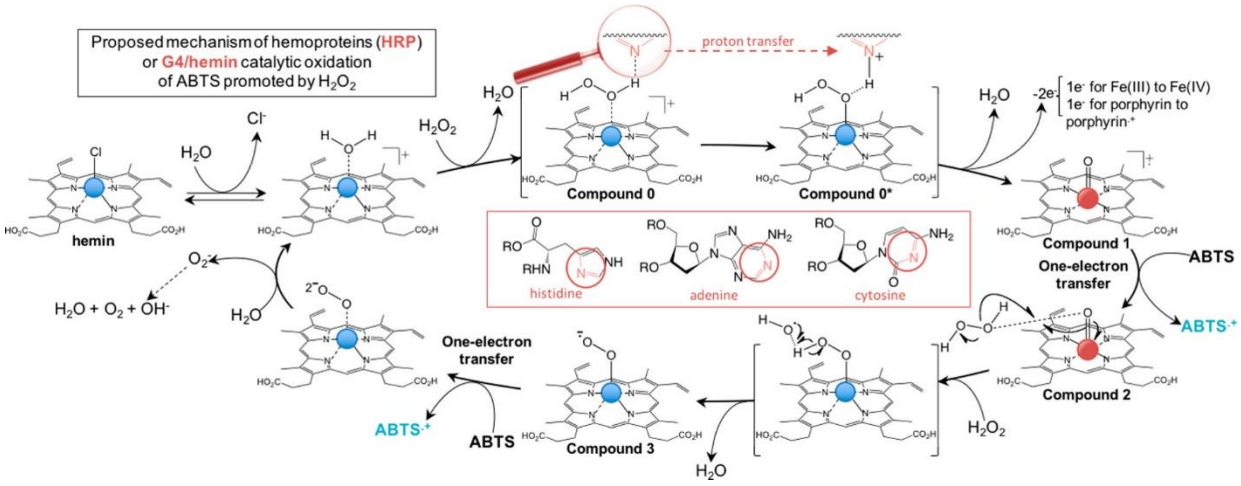

Figure 4: Proposed peroxidation mechanism by G4 with $ABTS^{2-}$ in the presence of hemin and H_2O_2.[31] The blue sphere represents Fe^{3+} while the red sphere represents Fe^{4+}. The proximal nucleotide assists with the proton transfer, which promotes the formation of Compound 1. Compound 1 then participates in oxidation-reduction reaction with $ABTS^{2-}$ to produce $ABTS^{+}$·, which generates the green color visible by the naked eye. Reprinted with permission from ref 31. Copyright 2018 American Chemical Society

Previous literatures have shown that the peroxidase-like activity of the G4-hemin complexes can be enhanced by the presence of certain sequences in the loop or flanking regions of the G4.[31-35] Specifically, Chen et al., proposed that the presence of adenine or cytosine in the vicinity of the hemin-binding site has the capability to facilitate the proton transfer step (Figure 4).[31] This accelerates the formation of Compound 1 and enhances the catalytic activity of the G4.[31]

The ability of G4-hemin complex to oxidize a colorless reagent into a colored product has been successfully integrated in a binary probe design, one of which is the sPDz.[9,26,28] sPDz is composed of two probes, and each has an arm that is complementary to the target sequence.[9,26,28] Each probe's "arm" is connected to a G-rich fragment, which will be used to form the G4 structure.[9,26] When designing the probes, two types of probes, U and S, are considered.[9] The purpose of the "U" probe is to unwind the target structure, while the purpose of the "S" probe is for selectivity.[9] For the S probe to be selective at room temperature, its target-binding arm is designed to be short - (7-10) nucleotides.[28] A short arm makes it energetically unfavorable to hybridize when SNP is present.[28]

In the presence of the target, the two strands will hybridize with the complementary sequence (Figure 5).[9] Then, the G-rich sequences will be in proximity of each other, allowing the G4 to form in an intermolecular manner.[9,26,28,36,37] When H_2O_2 and hemin are introduced into the environment, the G4-hemin complex will be able to catalyze the oxidation of $ABTS^{2-}$ (or another chromogenic substrate) to form a colored product.[9,36]

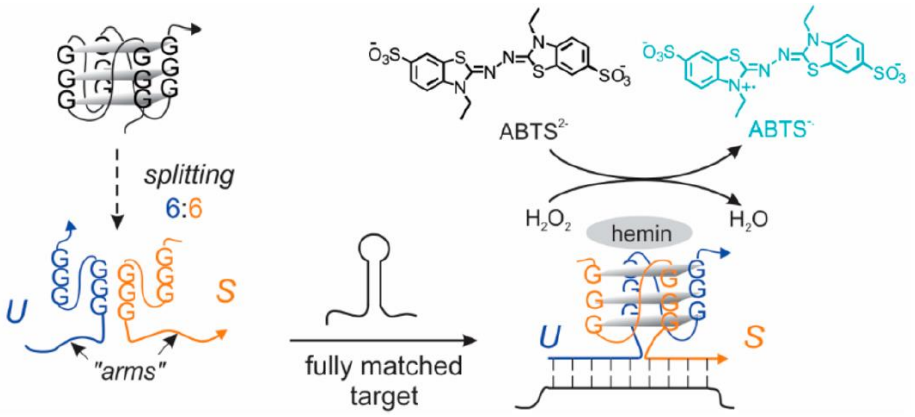

Figure 5: Approach to designing Split PDz probes and the Mechanism of signal generation.[9] Reprinted with permission from ref 9. Copyright 2019 American Chemical Society

Previous literatures have shown that the splitting methods can impact the performance of the intermolecularly formed G4 of the probes.[9,36,37] Connelly et al., proposed an algorithm that guides for the splitting method (i.e., 3:9, 6:6, 9;3) depending on the presence of G or C clusters in the target as well as the presence of a single nucleotide substitutions.[9] Such algorithm provides a roadmap for the optimization of a sPDz even in a complex situation with a number of varying factors.[9] Most splitting methods are usually in multiples of 3. However, Zhu et al. proposed that a 4:8 split of the 12 Gs from the 5' end provides a favorable signal to background ratio as well.[37] These distribution manners were considered in the present work when constructing the optimal probes for detection.

Binary Deoxyribozymes with Catalytic Core, and Its Applications for Colorimetric Assay.

In 1997, Santoro and Joyce reported of two RNA-cleaving deoxyribozymes with 8-17 and 10-23 catalytic motifs.[38] In the presence of a RNA target, these deoxyribozymes will hybridize and position its catalytic core in proximity of a cleavage site to enable efficient cleavage of a RNA phosphodiester bond.[38]

Based on the two unimolecular RNA-cleaving deoxyribozymes found by Santoro and Joyce, Mokany et al., reported binary deoxyribozymes called MNAzymes.[39]

In this binary probe design, there are two strands that include arm for a fluorogenic substrate binding, and a sensor arm that can detect an analyte (e.g. a target DNA/RNA).[39] Here, the fluorogenic substrate is a DNA oligonucleotide containing ribonucleotides as a cleavage site.[39] In addition, it includes a fluorophore and a quencher attached at the opposite sides of the DNA oligonucleotides. In the presence of the target, the two strands will hybridize to the target

using their sensor arms.[39] When the two strands of the split deoxyribozyme are in proximity, the catalytic core can form, and cleave the substrate that binds to the substrate arms of the two strands.[39] This innovative design provides an alternative method for development of biosensors.

Most deoxyribozyme sensors based on the MNAzyme model depend on fluorescence as signal.[26,39] However, a fluorometer is required to read the fluorescence signal, which may be a barrier when developing an effective point-of-care test.[8,39] Therefore, a colorimetric assay that utilizes the deoxyribozyme sensors is favorable as the signal can be read by the naked eye.[9] Previous literature reports have shown that such design is possible through a combination of 10-23 based split RNA-cleaving deoxyribozyme (sDz) with a peroxidase-like deoxyribozyme (PDz) cascade system.[40,41]

The split deoxyribozymes in the cascade system were designed so that each strand of the deoxyribozyme has two arms: (1) target-binding arm; (2) Inhibited peroxidase-like deoxyribozyme (IPDz) binding arm (Figure 6).[40,41] In the presence of the target, the sDzs will bind to it and form a catalytic core.[40,41] Then, the IPDz-binding arm will hybridize to the IPDz, and the catalytic core will cleave it, releasing an unimolecular sequence that can form a G4.[40,41] In the presence of hemin, the G4 will catalyze the oxidation of $ABTS^{2-}$ (or an alternative chromogenic dye, such as diamino benzidine (DAB)) to its colored product, producing a visual signal.[40,41]

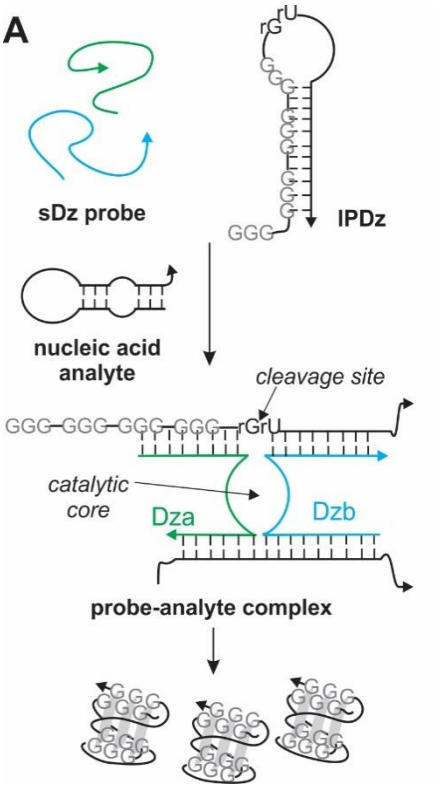

Figure 6: *The mechanism behind sDz/PDz cascade. The presence of the analyte allows the two strands of the sDz probe to form a catalytic core. The catalytic core is then able to cleave the IPDz and release G4 structure, producing a color change in the presence of hemin and a chromogenic substrate. This image is a courtesy of Dr. Yulia Gerasimova*.

The IPDz was designed to form a stem-loop structure to prevent a high background signal. Without the stem-loop structure, the G-rich sequence in the IPDz structure will be able to form a G4 region in the absence of the analyte, causing a high background signal. In addition, the melting temperature of the IPDz structure must be considered, as a melting temperature that is much lower than the assay temperature can lead to high background signal even in the absence of the target due to the destabilization of the structure. This can facilitate the formation of G4 regardless of the target's presence.

As the cascade system and the sPDz do not require an expensive machine to read the sign, they may be promising assays for a POC.[8]

METHODOLOGY

Materials

Oligonucleotides used in this study were all purchased from IDT, Inc. The design of MP_T60 was based on the paper by Li et al.,[24.]

Table 1: Sequences of Synthetic Targets.

Name	Sequences
MP_T60	TAAAGACAACGAATACAGAAGCCGTAATCTATGTTGTCTATCGTGTCCTC CGGGAACTTA
CPOX_T 60	TAAAGACAACGAATACA**A**A**C**GCC**A**T**C**ATCTATGTTGT**T**TATCGTGTCCTC CGGGAAC**A**TA
VCV_T6 0	TAAAGACAACGAATACA**A**A**C**GCC**A**TAAT**T**T**G**TGTTGT**T**TATCGTGTCCT CCGGGAAC**A**TA
VARV_T 60	TAAAGACA**C**CGAATACA**A**A**C**GCC**A**TAATCT**G**TGTTGT**T**TATCGTGTCCT CCGGGAAC**A**TA

Mismatching sequence when comparing MP_T60 to other Orthopoxviruses sequences are bolded in red.

Table 2: Primers

Name	Sequences	T_m (°C)
FP	GGAAAGTGTAAAGACAACGAATACAG	63.2
RP-A	GCTATCACATAATCTGAAAGCGTA	61.8
LATE-RP-1	CATTGTGTATTAGTCTTGCTATCACATAATCTGAAAGCGTA	70.1
LATE-RP-2	GCTATCACATAATCTGAAAGCGTAAGTTCCCGG	70.9
LATE-RP-3	GCTATCACATAATCTGAAAGCGTAAGTTCCC	68.2

T_m was calculated using Thermo Fisher T_m calculator with Phusion or Phire DNA Polymerase setting. 0.5µM was used for primer concentration.

Colorimetric Assay based on sPDz Probes and Synthetic Targets

Each sample was prepared to a volume of 60 μL at a temperature of ~22°C using a colorimetric buffer (50 mM HEPES-NaOH, pH 7.4, 20 mM KCl, 50 mM $MgCl_2$, 120 mM NaCl, 1% v/v DMSO, 0.03% v/v Triton X-100). It contained MP_T60 (1 μM) (excluding blank samples for negative control) and sPDz probes (1 μM each). 1.5 μL of a solution containing 15 μM Hemin and 40 mM $ABTS^{2-}$, and 0.6 μL of 100 mM H_2O_2 were added to each sample and vortexed and centrifuged. Following a 5-minute incubation period at ~22°C, the absorbance measurements of the samples were measured with NanoDrop One^C at 420 nm. For selectivity tests, CPOX_T60, VCV_T60, and VARV_60 (all at 1 μM) were used.

Polymerase Chain Reaction (PCR)

Genomic DNA from Monkeypox Virus, hMPXV/USA/MA001/2022 (Lineage B.1, Clade IIb) was used as a template DNA. Each sample consisted of 1X Phusion Flash PCR Master Mix (Thermo Fischer Scientific Inc.) 0.5 μM of forward primer and either 0.5 μM (for symmetric PCR) or 0.05 μM (for asymmetric PCR) of reverse primer. Negative control contained DNAse-free water while other samples contained 4.125×10^{-4} ng/µL of template DNA. Amplification was done via BioRad C1000 thermocycler with the following steps: (1) initial denaturation of DNA template [98°C for 3 min] (2) Denaturation [98°C for 10 secs] (3) Annealing [62°C for 10 secs] (4) Extension [72°C for 10 secs] (5) Final extension [72°C for 1 min]. Steps (2) to (4) were repeated 45 times before the final extension step.

Colorimetric Assay based on sPDz Probes and PCR Amplicons

Each sample was prepared to a volume of 60 μL at a temperature of 22°C using a colorimetric buffer (50 mM HEPES-NaOH, pH 7.4, 20 mM KCl, 50 mM $MgCl_2$, 120 mM NaCl, 1% v/v DMSO, 0.03% v/v Triton X-100). It contained 10 μL of diluted PCR amplicons (excluding blank samples for negative control), and 1µM sPDz probes. For trial 1, 11.7% (v/v) was PCR amplicons, while for trial 2, 15% (v/v) was PCR amplicons. The samples were annealed at a temperature of 94~95°C for 2 minutes and cooled down at room temperature for 10 minutes. Then, 1.5 μL of a solution containing 15 μM Hemin and 40 mM ABTS, and 0.6 μL of 100 mM H_2O_2 were added to the samples and vortexed and centrifuged. Following a 5-minute incubation period at 22°C, the absorbance measurements of samples were measured with NanoDrop One^C at 420 nm.

Colorimetric Assay based on sDz and PDz cascade and PCR Amplicons

For 60 μL Samples: Samples were initially prepared to 50 μL with the colorimetric buffer (50 mM HEPES-NaOH, pH 7.4, 20 mM KCl, 50 mM $MgCl_2$, 120 mM NaCl, 1% v/v DMSO, 0.03% v/v Triton X-100) at a temperature of ~22 °C. Each contained 1 μM of IPDz substrate with 0.1 μM of each corresponding Dza and Dzb strands. Then, 10 μL of either water (for blanks) or PCR products were added to the 50 μL sample. These were then incubated at 55°C for 50 minutes, followed by a 5-minute cooling period at ~22°C. Next, 1.5 μL of a solution containing 15 μM Hemin and 40 mM ABTS, and 0.6 μL of 100 mM H_2O_2 were added to each sample and vortexed and centrifuged. The samples were incubated for ~5-6 minutes at ~22°C. Then, their absorbance was measured at 420 nm using NanoDrop One^C spectrophotometer.

For 30 μL Samples: Samples were prepared to 30 μL with colorimetric buffer (50 mM HEPES-NaOH, pH 7.4, 20 mM KCl, 50 mM $MgCl_2$, 120 mM NaCl, 1% v/v DMSO, 0.03% v/v Triton X-100) at a temperature of ~22 °C. Each contained 1 μM of IPDz substrate with 0.1 μM of each corresponding Dza and Dzb strands. Of the 30 μL, 5 μL was either water (for blanks) or PCR products. These were then incubated at 50°C for 1 hour, followed by a 10-minute cooling period at ~22°C. Next, 1 μL of a solution containing 11.8 μM Hemin and 31.5 mM ABTS, and 0.5 μL of 63 mM H_2O_2 were added to the sample and vortexed. The samples were incubated for 5 minutes at ~22°C. Then, their absorbance was measured at 420 nm using NanoDrop One^C spectrophotometer.

Gel Electrophoresis Analysis

The obtained products of PCR were analyzed using ~3% agarose gel. 5µL or 10µL of the PCR amplicons were used per lane for Gel Electrophoresis Analysis. Gel electrophoresis were performed in 1X TAE buffer, and samples were run at 80V. The agarose gel contained either 0.6 or 1X GelRed. The gel pictures were obtained via BioRad Gel Doc XR+ System and the Image Lab software.

Fluorescence Assay

Samples of 60µL were prepared using a colorimetric buffer (50 mM HEPES-NaOH, pH 7.4, 20 mM KCl, 50 mM $MgCl_2$, 120 mM NaCl, 1% v/v DMSO, 0.03% v/v Triton X-100). Each sample contained 200 nM of FAM substrate, 30 nM each of Dza and Dzb. A positive control of 5 nM synthetic MP_T60, and a negative control with 6µL of water was prepared. Other samples contained 6µL of PCR products. All samples were incubated at 55°C for 1 hour and then measured using the Agilent Cary Eclipse Fluorescence Spectrophotometer. The emission value at 517 nm was used for data analysis. The excitation wavelength was 485 nm.

Outlier Calculation

Outlier calculation was done using GraphPad online calculator. The significance level of alpha=0.05 was used for calculation purposes.

OBJECTIVE

The objective of this study is to develop split PDz probes and sDz/PDz cascade system that can detect Mpox genetic signatures and provide a high signal. In addition, we aimed to optimize the sPDz probes to be selective enough to distinguish the targeted sequence of Mpox from that of other viruses in the same family.

RESULTS

Designing and Optimizing sPDz Probes

The first set of sPDz probes, shown below in Table 3, was designed by varying two factors: (1) splitting of the G4 forming region; (2) variation of loops or adding flanking sequences. G4 splitting positions (9:3, 6:6, 3:9, and 4:8) found in current literatures were used.[9,36,37] In addition, loops containing ATT and flanks composed of TC were tested as these were reported to enhance the catalytic ability of a unimolecular G4.[31,32] When designing these probes, NUPACK program was used to predict the secondary structure of the synthetic target sequences (MP_T60, Table 1).[42] The predicted secondary structure of MP_T60 and the target's fragments interacting with probes U and S (referred to in the text as the pair of probes) of the probes are shown in Figure 7.

Table 3: Oligonucleotide sequences of the first set of the sPDz probes.

Pair	Name	Sequences
1	U1-G9-TT-TT-*TT*	GGGTTGGGTTGGGTTTAGACAACATAGATTACGGCTT
	S1-G3-*TT*-TC	CGGAGGACACGATTGGGTC
2	U1-G4-TT-*TT*	GTTGGGTTTAGACAACATAGATTACGGCTT
	S1-G8-*TT*-TTT-ATT	CGGAGGACACGATTGGGTTTGGGATTGG
3	U1-G9-TTT-ATT-*TT*	GGGTTTGGGATTGGGTTTAGACAACATAGATTACGGCTT
	S1-G3-*TT*-TC	CGGAGGACACGATTGGGTC
4	U1-G4-T-*TT*	GTGGGTTTAGACAACATAGATTACGGCTT
	S1-G8-*TT*-T-T	CGGAGGACACGATTGGGTGGGTGG
5	U1-G6-TT-TT-*TT*	TTGGGTTGGGTTTAGACAACATAGATTACGGCTT
	S1-G6-*TT*-TT-TC	CGGAGGACACGATTGGGTTGGGTC

Highlighted (yellow) sequences represent G4 forming region; blue represent either the flanking or the loop sequences; purple represents linker sequences; red represents the "arms" of the probes that bind to the synthetic target MP_T60.

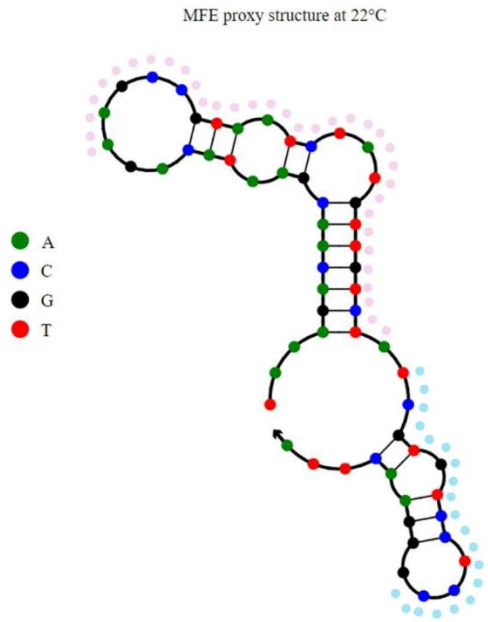

Figure 7: Secondary structure of MP_T60 predicted by NUPACK.[42] The pink dotted line represents the region of the synthetic target bounded by the U1 strands, and the blue dotted line represents the region bounded by the S1 strands.

These pairs of probes were first tested with the synthetic target MP_T60, and the signal-to-background (S/B) value was computed by dividing the absorbance measurement at 420 nm of the sample containing 1μM of MP_T60 with that of the sample absence of MP_T60 (blank). The average of these S/B values from each trial for each pair of probes is shown in Figure 8. From here, we were able to determine that Pair 5 (U1-G6-TT-TT-*TT* & S1-G6-*TT*-TT-TC) provided the highest average S/B. Therefore, 6:6 splitting of the G4 forming region was utilized for sDPz designs that target MP_T60.

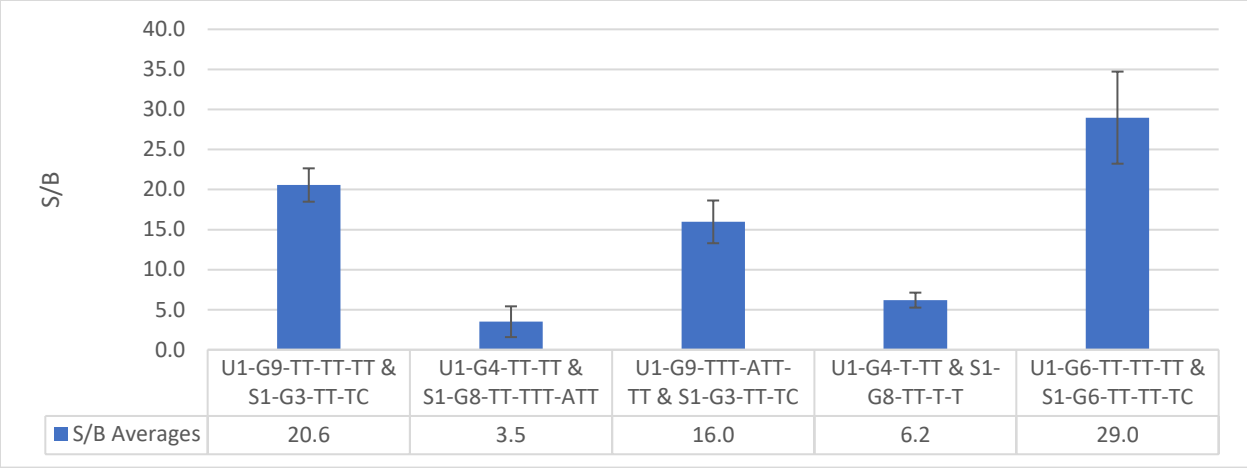

Figure 8: Averages of S/B for each pair of the sPDz probes. S/B for each trial was computed and then averaged across all trials. Three or four trials were done for each pair of probes.

U1-G6-TT-TT-*TT* & S1-G6-*TT*-TT-TC pair was then further tested with synthetic targets of other Orthopoxviruses (i.e., CPOX_T60, VCV_T60, VARV_T60) for selectivity test. The selectivity was measured using the selectivity factor (SF). SF was computed using the equation shown below.

$$\mathrm{SF} = \left[1 - \frac{\mathrm{A_{OT}} - \mathrm{A_0}}{\mathrm{A_T} - \mathrm{A_0}}\right] \times 100\%$$

(Equation 1).

where $\mathrm{A_{OT}}$, $\mathrm{A_0}$, and $\mathrm{A_T}$ represents the absorbance at 420 nm for samples containing off-targets (e.g., CPOX, VCV, VARV), no-target, and the fully complementary target MP_T60, respectively. Table 4 shows U1-G6-TT-TT-*TT* & S1-G6-*TT*-TT-TC pair's average SF. For SF with VCV_T60, an outlier was detected from the three trials conducted; therefore, analysis was done from the data of the two other trials. Based on the standards set by the literature, a SF ≥ 90 indicates a sufficient probe performance. [9]

Table 4: Average *of SF between Mpox and one other Orthopoxvirus across two to three trials for U1-G6-TT-TT-TT & S1-G6-TT-TT-TC Pair.*

	SF with VCV_T60	SF with CPOX_60	SF with VV_T60
Average	87±1	39±14	35±23

The data reflects U1-G6-TT-TT-*TT* & S1-G6-*TT*-TT-TC pair's insufficient ability to be selective, with all average SF values below 90. Provided that the end goal of this assay was to be efficient enough to be incorporated in POCTs, we determined that the probes had to be redesigned.

Based on the 6:6 split of U1-G6-TT-TT-*TT* & S1-G6-*TT*-TT-TC and with the goal to improve selectivity, new designs were developed. To improve the probe's selectivity, the target region for probes was shifted so that the region of interrogation by probe S included nucleotide variations between the synthetic targets of Mpox and other Orthopoxviruses. In addition, the arm of probe S was shortened with the purpose that a stable probe target hybrid at the assay temperature (~22°C) is only formed with the fully complementary target (Figure 9). Shorter arm length improves selectivity as even one mismatch becomes more energetically costly. High performing probes' sequences are shown below in Table 5.

Table 5: *Oligonucleotide sequences of the second set of sPDz Probe.*

Name	Sequences
sPDz "U"	
U2-G6-*T*-TT-TC	ACGATAGACAACATAGATGGGTTGGGTC
U2-G6-TT-TC	ACGATAGACAACATAGAGGGTTGGGTC
sPDz "S"	
S2-G6-TT-*T*	GGGTTGGGTTTACGGCTTC
S2-G6-ATT-TT-*T*	ATTGGGTTGGGTTTACGGCTTC
S2-G6-TT-*T*+*T*	GGGTTGGGTTTACGGCTTCT
S2-G6-TT	GGGTTGGGTTACGGCTTC

Highlighted (yellow) sequences represent G4 forming region; blue represent either the flanking or the loop sequences; purple represents linker sequences; red represents the "arms" that bind to the synthetic target.

Out of these probes, the following combinations were tested: (1) U2-G6-*T*-TT-TC & S2-G6-TT-*T* (2): U2-G6-*T*-TT-TC & S2-G6-ATT-TT-*T* (3) U2-G6-*T*-TT-TC & S2-G6-TT-*T*+*T* (4) U2-G6-TT-TC & S2-G6-TT. A selectivity test was performed for the combination that had the highest S/B average across four trials (Figure 10), which was combination (2) U2-G6-*T*-TT-TC & S2-G6-ATT-TT-*T.* The result for the selectivity test is shown in table 6. For SF with VCV_T60, an outlier was detected from the three trials conducted; therefore, analysis was done from the data of the two other trials.

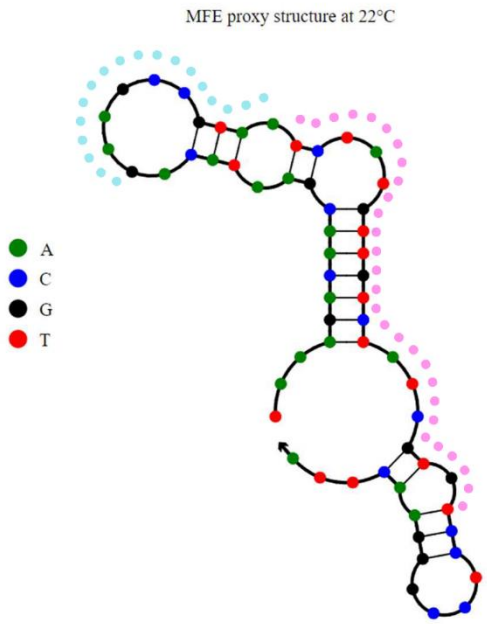

Figure 9: Secondary structure of the MP_T60 predicted by NUPACK.[42] The pink dotted line represents the region of the synthetic target bounded by the U2 probe, and the blue dotted line represents the region bounded by the S2 probe.

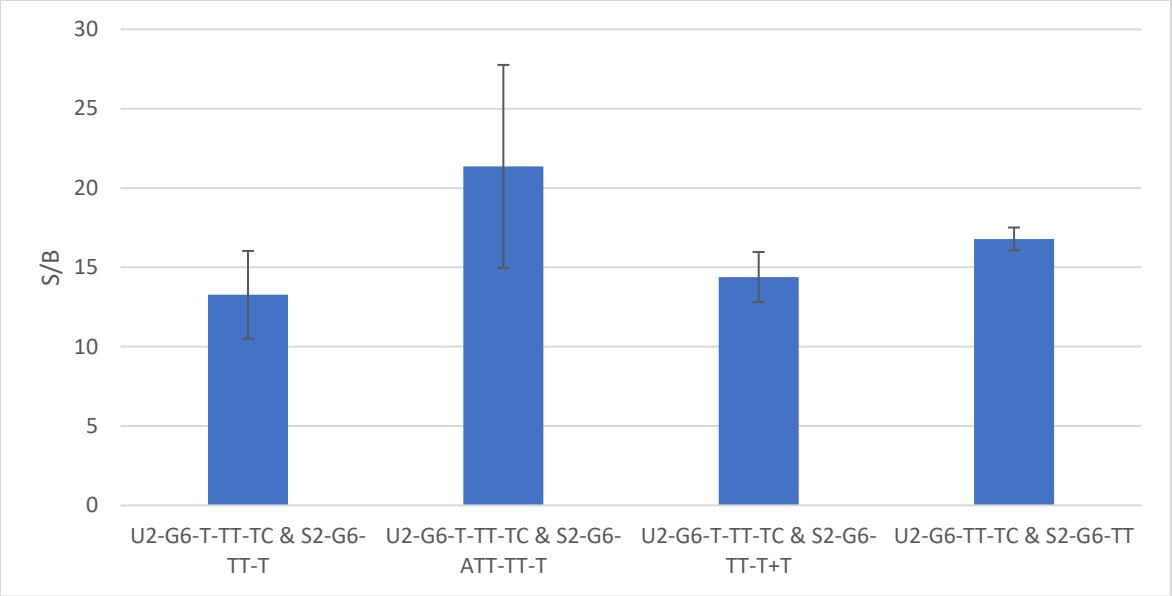

Figure 10: Averages of S/B for the sPDz probes composed of the indicated U and S probes. S/B for each trial was computed and then averaged across all trials. Four trials were done for each pair of probes.

*Table 6: Average and Standard Deviation of SF between Mpox and one other Orthopoxvirus across two to three trials for (2) U2-G6-*T*-TT-TC & S2-G6-ATT-TT-*T.

	SF with VCV_T60	SF with CPOX_60	SF with VV_T60
Average	99.5±0.5	100*	99.6±0.3

*If the SF value was greater than 100, it was readjusted to 100. This occurs when the absorbance measurement in the sample containing off-targets is lower than the measurement of the sample absence of the target (blank).

The data from the selectivity test for U2-G6-*T*-TT-TC & S2-G6-ATT-TT-*T* combination confirmed its high selectivity. Unlike the U1-G6-TT-TT-*TT* & S1-G6-*TT*-TT-TC pair, U2-G6-*T*-TT-TC & S2-G6-ATT-TT-*T pair* had an SF all greater than 99.

Polymerase Chain Reaction and Fluorescence Assay

To further assess the probe's ability to detect Mpox genetic signatures, we decided to test it with PCR amplicons. This is because many nucleic acid-based tests utilize PCR or other amplification mechanisms to increase the copy of low-abundant DNA targets present in clinical samples. PCR was performed both symmetrically and asymmetrically. Symmetrical PCR uses equal concentration of reverse and forward primers, while asymmetrical PCR uses unequal concentrations. Genomic DNA from Monkeypox Virus, hMPXV/USA/MA001/2022 (Lineage B.1, Clade IIb) supplied by BEI resources served as a template DNA.

Asymmetrical PCR, specifically the LATE (Linear-After-The-Exponential)-PCR[43], was done with the goal of producing single stranded DNA (ssDNA) amplicon, which is hypothesized to improve the efficiency of probe's ability to bind to the target. Asymmetrical PCR requires that the concentration of one of the two primers is lower than that of the others.[43] Such condition allows ssDNA to be generated once the limiting primer is exhausted. For this project, the ratio of forward-to-reverse primers was 10:1. In addition, LATE-PCR requires that the concentration-adjusted limiting primer's T_m is greater than that of the excess primer to ensure that efficient annealing occurs.[43]

The design of the primers was based on the CDC's Test procedure for Monkeypox virus Generic Real-Time PCR Test.[24,25] For LATE reverse primers, their 3'- or 5'-ends were elongated to increase their T_m. The combinations of forward and reverse primers that were tested are shown in Table 7. To determine the most optimal asymmetrical PCR primer combinations, fluorescence assay was performed using split deoxyribozyme. The split deoxyribozyme for the fluorescence assay was designed so that each strand's arm interrogated a fragment in the middle of the

amplicons (Table 8). Therefore, an increase in fluorescence was expected if the PCR was able to successfully amplify the target sequence of interest. In addition, if a higher number of PCR amplicons were produced, a higher fluorescence was expected. Three trials were performed with PCR samples that had 3.3×10^{-5} µg/µL of genomic DNA from Monkeypox Virus, hMPXV/USA/MA001/2022 (Lineage B.1, Clade IIb) as the template DNA. Results are shown in Table 9.

Table 7: List of combinations of PCR primers that were tested.

Combination Name	Forward Primer	Reverse Primer	PCR Type
S	FP	RP-A	Symmetrical
1A	FP	LATE-RP-1	Asymmetrical
2A	FP	LATE-RP-2	Asymmetrical
3A	FP	LATE-RP-3	Asymmetrical

Table 8: *Sequences for the strands of the Split deoxyribozyme probe used in MP-T60-specific fluorescence assay.*

Name	Sequences
FAM Fluorogenic Substrate	AAGGT-(dT-FAM)-TCCTCguCCCTGGGCA-(BHQ 1)
MP_sDz_S	**CCGGAGGACACGATA** *ACAACGA* GAGGAAAACCTT
MP_sDz_U	TGCCCAGGGA *GGCTAGCT* **GACAACATAGATTACGGCTT**

*The sequences in orange represent arm of deoxyribozyme targeting the fluorogenic substrate; bolded sequences represent arm targeting the DNA of interest; italicized sequences represent the nucleotides forming

Table 9: *Fluorescence values for each sample. NTC represents PCR no-target-control while T represents PCR sample with Mpox template DNA.*

	Trial 1	Trial 2	Trial 3	Average
Blank (Negative control)	20.736	14.18	17.672	17.5
5 nM MP_T60	122.404	154.524	160.22	145.7
NTC-S	28.294	26.834	27.64	27.6
T-S	96.58	67.67	26.8	63.7
NTC-1A	26.275	30.218	26.551	27.7
T-1A	49.067	23.426	23.377	32.0
NTC-2A	28.266	30.62	24.441	27.8
T-2A	146.109	52.006	25.318	74.5
NTC-3A	25.368	25.762	24.37	25.2
T-3A	57.869	31.107	25.673	38.2

Although not all values in Trial 3 were outliers when analyzed with trials 1 and 2, their values were not considered in evaluating performance of the primers as the values of NTC and T were similar even for symmetric PCR. Based on the result shown in Table 9, we were able to determine combination 2A (FP & LATE-RP-2) as the most optimal primer combinations among the asymmetrical PCR primers.

Based on the result shown in Table 9, we decided to select combination 2A to perform an additional two trials of PCR but with higher template DNA concentration (4.125×10^{-4} ng/µL) for the purpose of producing more amplicons to test with sPDz and sDz/PDz cascade system. Analysis of the PCR amplicons of two independent PCR trials using agarose gel electrophoresis is shown in Figure 11.

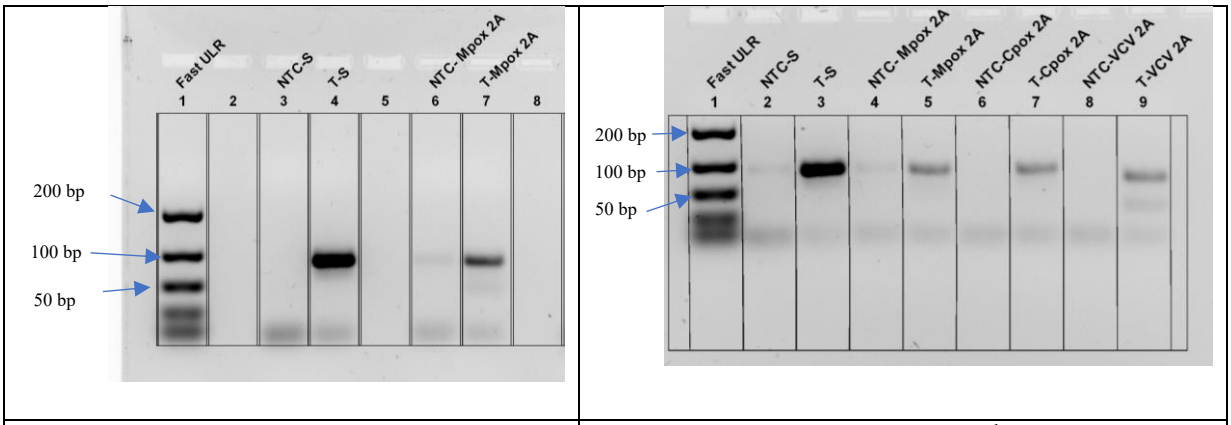

Gel Picture from 1st trial | Gel picture from 2nd trial.

Figure 11:3% Agarose Gel pictures from 1st and 2nd trial of PCR. Both trials included the following components: (1) Fast ULR (Ultra Low Range) Ladder (2) NTC-S (3)T-S (4) NTC-Mpox 2A (5)T-Mpox 2A. The second trial includes the following additional components; (7) NTC-Cpox-2A (7)T-Cpox 2A (8) NTC-VCV-2A (9)T-VCV-2A. T represents the presence of template Mpox, Cpox, or VCV, DNA while NTC represents PCR no-target-control. 2A represents the usage of primer combination 2A (FP and LATE-RP-2) in an asymmetrical manner.

Based on the gel, we can observe that both the symmetric and asymmetric PCR produced amplicons of around 100 bp length; however, we were unable to determine, solely from the gel, if the asymmetric PCR method was able to produce ssDNA. In addition, we observed a similar

sized product, though much less intense for NTC in both trial 1 (NTC-Mpox-2A) and trial 2 (NTC-Mpox-2A and NTC-S). This may indicate contamination of the NTC sample.

Fluorescence assay was performed to determine if the target gene of interest was amplified with PCR (Figure 12). Based on the data, we can conclude that indeed the gene of interest was amplified through both symmetrical and LATE-PCR.

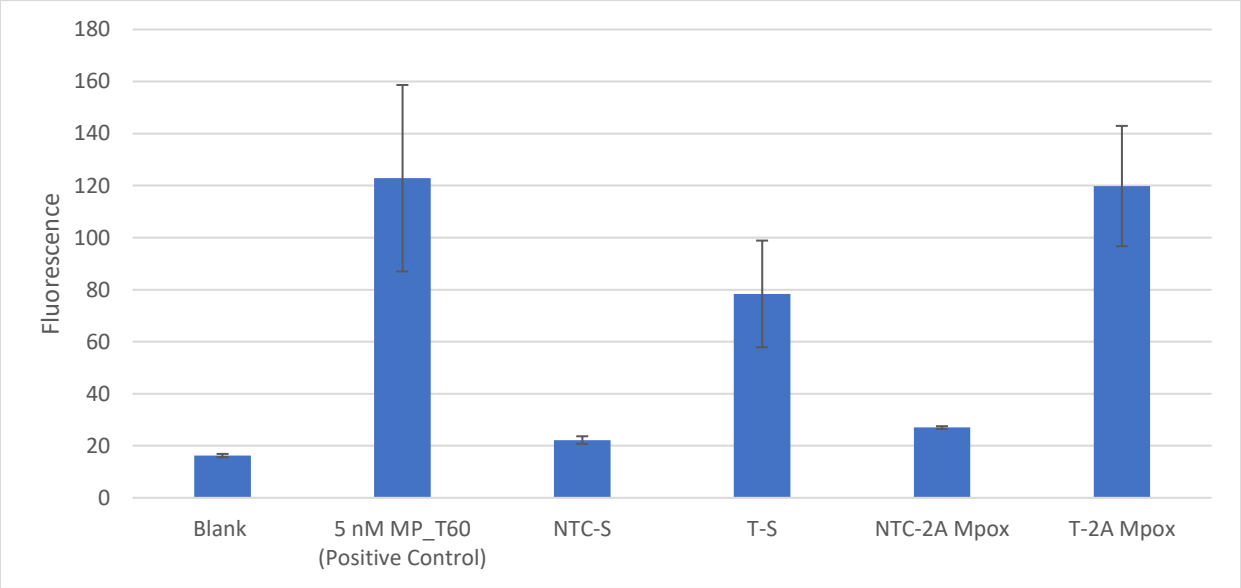

Figure 12: Average fluorescence values from two trials of indicated sample from fluorescence assay with sDz. PCR products produced from two independent PCR trials were used for NTC-S, T-S, NTC-2A Mpox, T-2A Mpox. Blank represents the no-target-control in the absence of the MP_T60. NTC-S and T-S represent the fluorescence of the sample containing products from the PCR no-target-control or target samples from symmetrical PCR, respectively. NTC-2A Mpox and T-2A Mpox represent the fluorescence of the sample containing products from the PCR no-target-control or target samples from LATE-PCR with FP & LATE-RP-2 as primers.

Testing of sDz/PDz Cascade with PCR Amplicons

Prior to testing the PCR amplicons with sPDz probes, we decided to test them with the cascade system first. The rational being that sDz/PDz cascades usually have a lower limit of detection (LOD) compared to sPDz probes.[26,40,44,45] The sequences for the sDz/PDz Cascade are shown in Table 10.

Table 10: Oligonucleotides used for sDz/PDz Cascade System.

Name	Sequences
IPDz-ATTT	GGG T GGG ATTT GGG T GGG TTC guC CAT GAG CACT CAAA TCC C
MPV-Dza-ATTT	GT GCT CAT GGA *GGCTAGCT* CAT AGA TTA CGG CTT CTG
MPV-Dzb-ATTT	CGGAGGACACGATAGACAA *ACAACGA* GAA CCC ACC C

*Sequences colored in red and sky-blue of the Dza and Dzb are the IPDz-binding arms that match the correspondingly colored complementary sequences on IPDz. The sequences that form the 10-23 catalytic core are in italics. Sequences colored in orange are the target-binding arms of Dza and Dzb. Sequences highlighted in yellow is the G4 forming region.

Trials were conducted from the amplicons generated from two independent PCR trials. Of the four sDz/PDz cascade trials, three were conducted with 50°C incubation for 1 hour with a samples volume of 30µL (Table 11). One trial was conducted with 55°C incubation for 50 minutes with a sample volume of 60µL (Table 11). In addition, given that the concentration of the probes, substrates, and buffer differed in the experiment of 30µL and 60µL, the data were analyzed separately. S/B was computed for each trial by dividing the absorbance measurement at 420 nm of the sample containing PCR amplicons by that of the corresponding PCR no-target-control. For positive control (0.1µM MP_T60), the blank (no-target-control in the absence of MP_T60) was used as the background.

Table 11: Absorbance values measured at 420 nm with sDz/PDz cascade. The green table represents the trials performed with 50 ℃ incubation for 1 hours with a sample volume of 30µL. The orange table represents the trials performed with 55 ℃ incubation for 50 mins with a sample volume of 60µL.

Absorbance at 420 nm after 50°C Incubation for 1 hours with a sample volume of 30µL					Absorbance at 420 nm after 55°C Incubation for 50 mins with a sample volume of 60µL
	Trial 1	Trial 2	Trial 3	Average	Trial 1
Blank	0.42	0.44	0.43	0.43	0.61
Positive Control	2.52	2.71	2.62	2.62	2.61
NTC-S	0.34	0.32	0.35	0.34	0.55
T-S	0.92	0.42	0.76	0.70	0.95
NTC-2A	0.43	0.39	0.44	0.42	0.53
T-2A	1.31	1.06	1.21	1.19	1.73

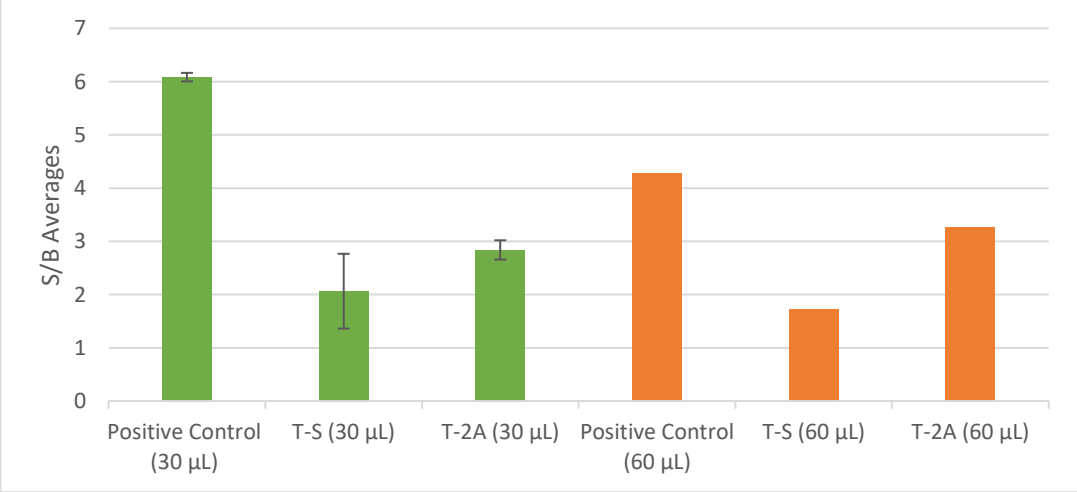

Figure 13: Averages of S/B for sDz/PDz Cascade system. The green bars represent the S/B averages of three trials conducted under 50 °C incubation for 1 hour. The orange bar represents the S/B from a single trial conducted under 55 °C incubation for 50 minutes. The S/B for positive control was calculated by dividing the absorbance measurement of sample containing 0.1 µM of MP_T60 with that of the sample absent of MP_T60 (blank). The S/B for T-S was calculated by dividing the absorbance measurement of the sample containing amplicons produced through symmetrical PCR with that of the symmetrical PCR-no-target-control. The S/B for T-2A was calculated by dividing the absorbance measurement of the sample containing amplicons produced through asymmetrical PCR with that of the corresponding asymmetrical PCR-no-target-control.

The S/B average for T-2A is 2.838, while that of T-S is 2.063. Although the S/B for the T-S and T-2A is lower than that of the positive control, their performance indicates that they can detect the genetic signatures of Mpox from the PCR amplicons.

Testing of sPDz Probes with PCR Amplicons

Once we confirmed that the sDz/PDz cascades were able to detect the PCR amplicons, we decided to test it with the most optimal sPDz probe (based on the highest S/B), which was U2-G6-*T*-TT-TC & S2-G6-ATT-TT-*T*. Two trials were conducted, and the S/B was computed for each trial. As with the sDz/PDz cascade trials, the PCR-no-target-control served as the background for PCR-target samples. In addition, the amplicons in both trials were diluted due to lack of PCR products. For Trial 1, 11.7% of the 60 μL was PCR amplicons while for Trial 2, 15% of the 60 μL was PCR amplicons. Since the concentrations of PCR amplicons differed, we decided to analyze the data separately for each sample per trial.

Based on the S/B values calculated from the experiments, it is difficult to conclude the effectiveness of sPDz. First, all the S/B of all trials were below 2. The only set that initially stood out was with T-2A (Trial 1), which the S/B was 1.84; however, in trial 2, the S/B was 1.12. Therefore, we are unable to state that the sPDz effectively detects the Mpox genetic signatures from PCR amplicons. This data suggests that sPDz was ineffective in targeting the gene fragments amplified by PCR with the current template concentration. This was expected as the template DNA concentration used for PCR was low (4.125×10^{-4} ng/µL).

Table 12: Absorbance values for sPDz Probes

Absorbance at 420 nm		
	Trial 1	Trial 2
Blank	0.26	
Positive Control	6.51	
NTC-S	0.24	0.25
T-S	0.27	0.24
NTC-2A	0.25	0.26
T-2A	0.46	0.29

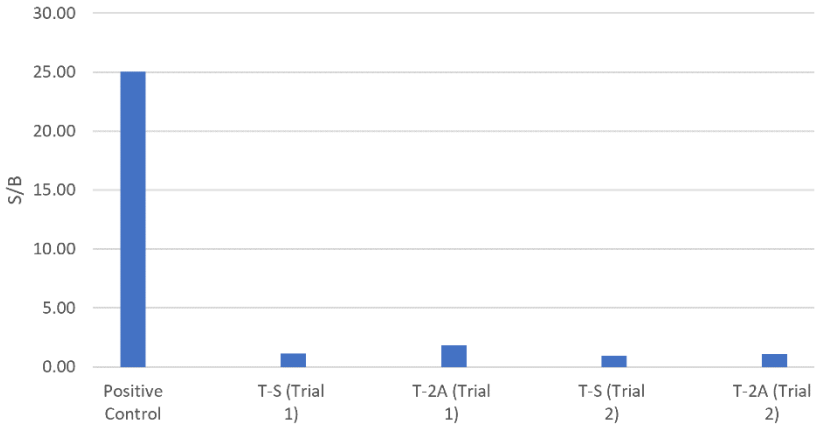

Figure 14: S/B values for sPDz Probes tested with the products of Mpox DNA amplified using PCR. S/B for each NTC and T set was calculated by dividing the absorbance measurement of the samples containing the PCR amplicons (T) with that of the PCR-no-target control (NTC). S/B for positive control was calculated by dividing the absorbance measurement of the sample containing 1µM of MP_T60 with that of the sample absent of MP_T60 (blank).

DISCUSSION

As with many other infectious diseases, the rise of the Mpox throughout the world alarmed the public health community. Although the number of cases has been decreasing in the past months, Mpox remains endemic in certain African nations. Therefore, cost-effective, and efficient point-of-care tests remain to be desired. To search for an answer to this problem, we explored different methods of assay development.

Through our experiments, we were able to show that the sDz/PDz cascade is able to successfully detect the Mpox genome fragments from Clade IIb amplified by PCR. Even though this signal was lower than one exhibited in the presence of 0.1μM MP_T60 serving as a positive control for the assay, it exceeded the absorbance of the blank and/or PCR no-template control 2-3-fold. We would like to acknowledge that the absorbance values for the blank (absence of MP_T60) and the positive control containing 0.1μM MP_T60 differed when another lab member performed the experiments. However, the S/B values were similar regardless of the experimentalist. In addition, given that the purpose of the experiment was to determine if the sDz/PDz cascade can detect the presence of the Mpox genetic signatures in the PCR amplicons, the conclusion did not change. Given that the cascade system was able to produce a signal with the PCR amplicons, and that it is a colorimetric assay-based test, it may be a suitable assay for a POCT. However, the sDz/PDz cascade system requires further work in multiple areas. First, the background's color intensity must be lowered to establish a clear difference in signal output between the presence and absence of the target (Table 11). The intensity of the blank in cascade assay was higher than 0.4 o.u, and was visually observed as a light or faint green color. When the output of the assay is read visually instead of relying on a spectrophotometer, this color can be

difficult to distinguish from the color of a sample containing low concentration of the target. The ideal system will have a colorless background, which the current cascade system does not. This can be done by optimizing the IPDz sequences to further sequester the G4 forming region as well as the sDz components of the cascade. Second, we will need to check the cascade's ability to be selective against other Orthopoxviruses. The selectivity can be initially evaluated by using the synthetic targets of other Orthopoxviruses.

Finally, the cascade system's limit of detection must be analyzed. Literatures analyzing the LOD of the cascade system were reported by Reed et al.,[44] Gerasimova et al.,.[40] and Dhar et al.[41] Reed et al. study with the zika virus showed that the cascade's LOD was approximately 1 nM.[44] Gerasimova et al., study with *Mycobacterium tuberculosis* showed that the cascade's LOD was approximately 0.4 nM with the synthetic target and using 3,3'-aiaminobenzidine as a chromogenic substrate.[40] The median viral load for Mpox in skin lesions was determined to be ~1.995×10^7 copies/mL ($7.3\log_{10}$).[46] This viral load corresponds to ~33fM viral DNA concentration, according to the equation below:

$$1.995 \times 10^7 \frac{\text{copies (molecules)}}{\text{mL}} \times 10^3 \frac{\text{mL}}{\text{L}} \times \frac{1 \text{ mol}}{6.022 \times 10^{23} \text{ copies (molecules)}}$$

Assuming the LOD of the Mpox-specific cascade system is similar to the values reported by Gerasimova et al., and Reed et al., it is obvious that amplification of the viral DNA is necessary to meet the LOD requirement. Therefore, increasing the amplicon's aliquot per sample for the sDz/PDz assay may improve the assay's performance in detecting genetic signatures of Mpox.

While the sPDz system was unable to reliably detect the PCR amplified fragments of the Mpox genome, it was successful in detecting the viral genetic signatures when synthetic DNA

targets were tested. In addition, we were able to optimize the probes to be selective. Therefore, upon additional optimization, it may have the ability to be used for Mpox screening.

In this study, we used both symmetrical and asymmetrical manner of PCR to amplify the gene of interest. By extending either the 3' or the 5' end of the limiting primer, we were able to raise its theoretical T_m (based on the Thermo Fisher Tm calculator) to balance the reduction of T_m with the lower concentration. Although we were unable to directly show that ssDNA was produced from the LATE PCR by using Gel electrophoresis analysis, the absorbance measurements with the cascade system suggests that it may have produced ssDNA. This is because the absorbance of the amplicon-containing samples using the sDz/PDz cascades was higher for amplicons produced by the asymmetrical PCR in comparison to the symmetrical PCR (Table 11).

To truly take this assay system to the next level, an isothermal amplification system should be sought as it will help reduce the cost of instruments required. Then, the sDz/PDz cascade system should be tested with the amplicons produced from this isothermal amplification system.

CONCLUSION

In this work, we were able to develop sPDz and sDz/PDz cascade systems that are both able to detect the presence of targeted Mpox genetic signatures in synthetic DNA targets. In addition, we were able to optimize the sPDz probes to be selective for the targeted sequence of the Mpox genome. With PCR, we were able to produce amplicons that included the target sequence of interest, which was confirmed by fluorescence assay with split deoxyribozymes. The sDz/PDz cascade system was able to detect the targeted Mpox genetic signatures in the PCR amplicons; however, the sPDz was unable to do so. Further works are necessary to optimize the cascade system to increase its signal while simultaneously lowering the background signal. For sPDz probes, they should be retested with a higher PCR amplicons concentration in the analyzed sample.

APPENDIX A
COPYRIGHT PERMISSIONS

Hello,

Thank you for reaching out about the graphic. I was able to find the graphic and attach it to this email. Here is the information I received from our headquarters about sourcing:

As we created the image ourselves, there are no copyright restrictions and we are free to let him use the image. Please find it attached. Could you let him know mention the source as follows?
INTEGRA Biosciences, https://www.integra-biosciences.com/en/blog/article/qpcr-how-sybrr-green-and-taqmanr-real-time-pcr-assays-work

If you have any further questions, please feel free to reach out in the chat.

Lizzy Vrettos
Content Manager
INTEGRA

INTEGRA Biosciences Corporation
22 Friars Drive
Hudson NH 03051
United States

Tel. +1 603 578-5800 (main)

Figure 15: *Permission for the usage of images in figures 1A and 1B from INTEGRA Biosciences Corporation.*

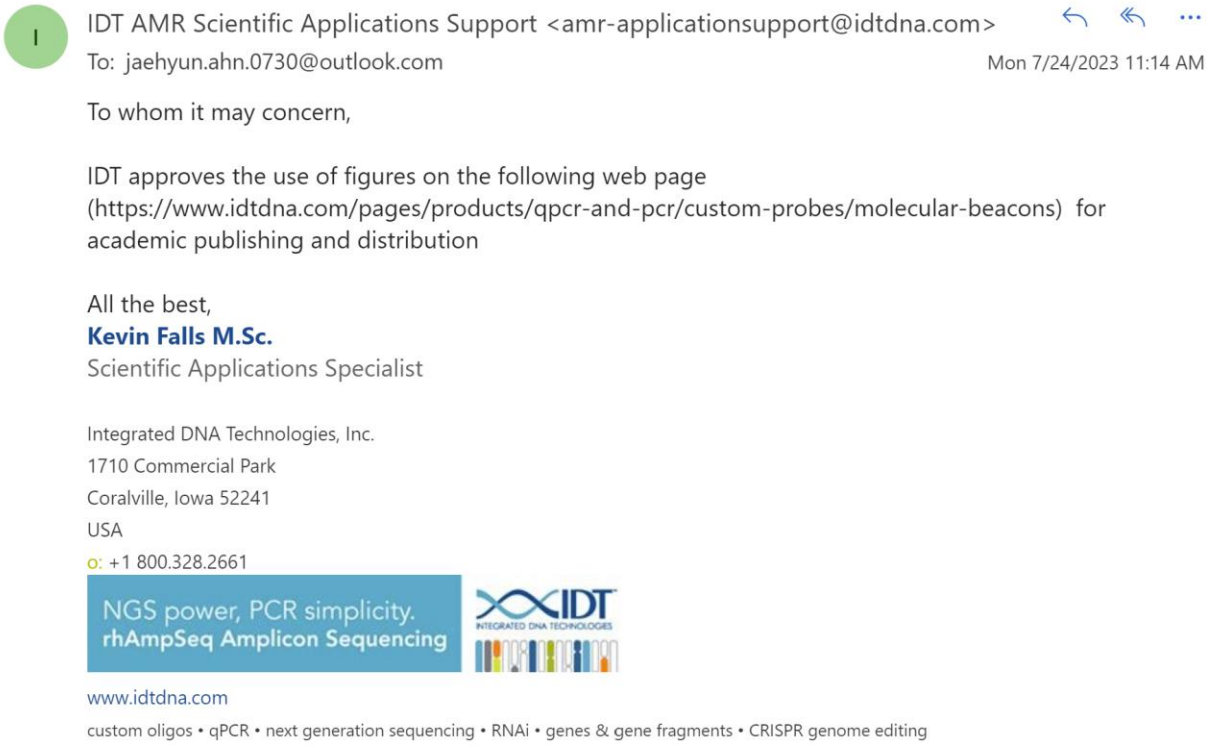

I

IDT AMR Scientific Applications Support <amr-applicationsupport@idtdna.com>

To: jaehyun.ahn.0730@outlook.com Mon 7/24/2023 11:14 AM

To whom it may concern,

IDT approves the use of figures on the following web page (https://www.idtdna.com/pages/products/qpcr-and-pcr/custom-probes/molecular-beacons) for academic publishing and distribution

All the best,

Kevin Falls M.Sc.

Scientific Applications Specialist

Integrated DNA Technologies, Inc.

1710 Commercial Park

Coralville, Iowa 52241

USA

o: +1 800.328.2661

www.idtdna.com

custom oligos • qPCR • next generation sequencing • RNAi • genes & gene fragments • CRISPR genome editing

Figure 16: Permission for the usage of images in figures 1C from Integrated DNA Technologies

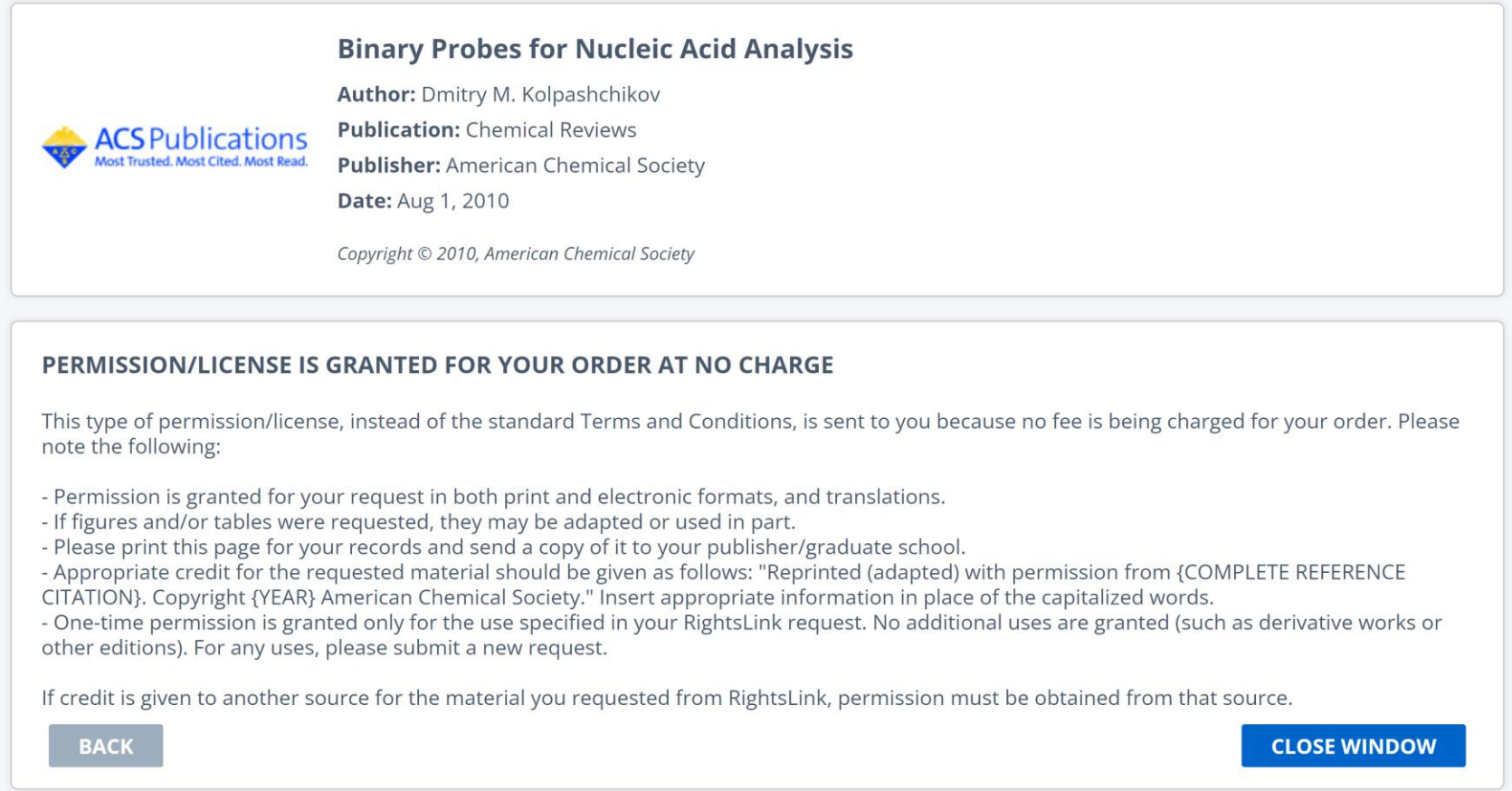

Figure 17: Permission for the usage of image in figure 2 from American Chemical Society.

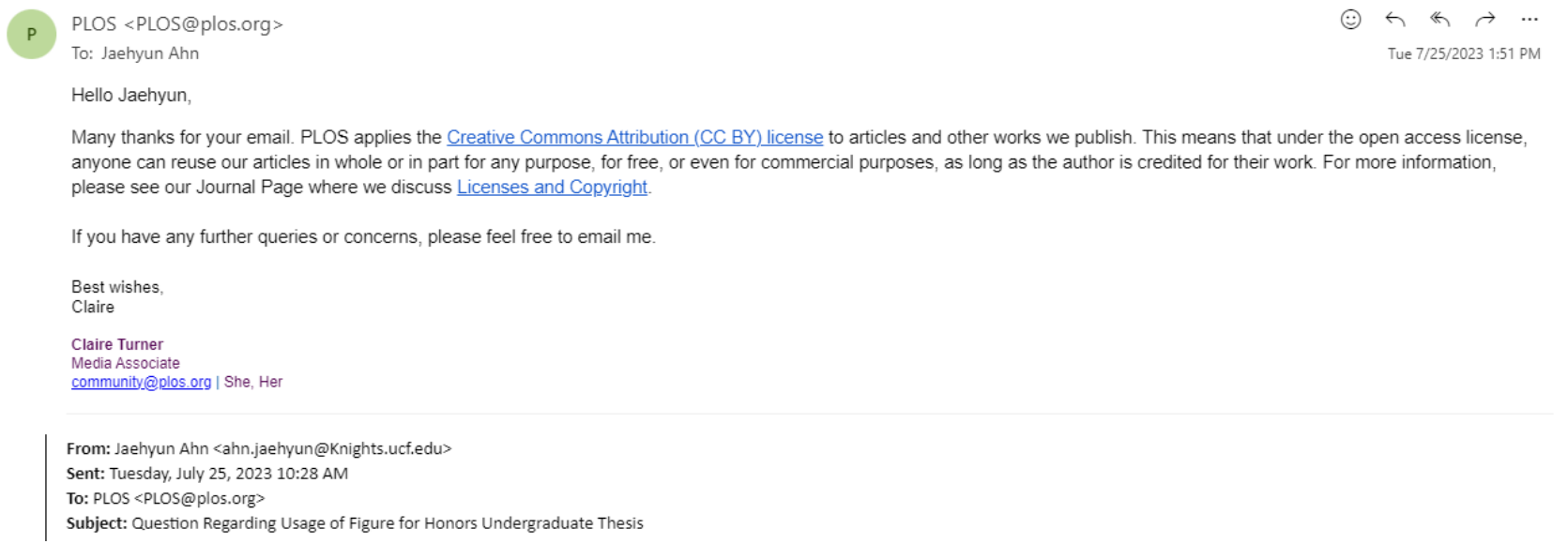

P

PLOS <PLOS@plos.org>

To: Jaehyun Ahn

Tue 7/25/2023 1:51 PM

Hello Jaehyun,

Many thanks for your email. PLOS applies the Creative Commons Attribution (CC BY) license to articles and other works we publish. This means that under the open access license, anyone can reuse our articles in whole or in part for any purpose, for free, or even for commercial purposes, as long as the author is credited for their work. For more information, please see our Journal Page where we discuss Licenses and Copyright.

If you have any further queries or concerns, please feel free to email me.

Best wishes,
Claire

Claire Turner
Media Associate
community@plos.org | She, Her

From: Jaehyun Ahn <ahn.jaehyun@Knights.ucf.edu>
Sent: Tuesday, July 25, 2023 10:28 AM
To: PLOS <PLOS@plos.org>
Subject: Question Regarding Usage of Figure for Honors Undergraduate Thesis

Figure 18: Statement from PLOS regarding the usage of image in figure 3

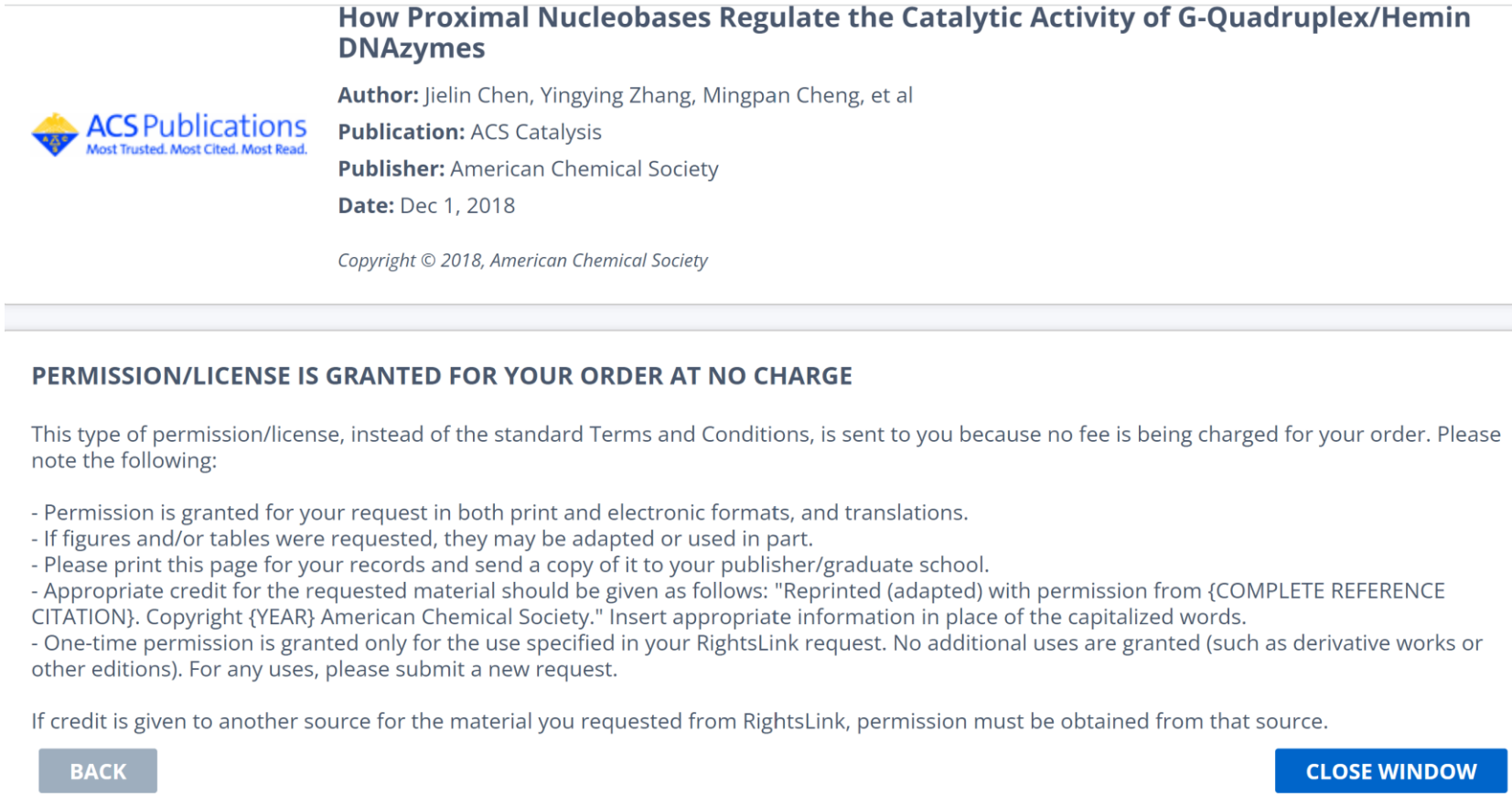

How Proximal Nucleobases Regulate the Catalytic Activity of G-Quadruplex/Hemin DNAzymes

Author: Jielin Chen, Yingying Zhang, Mingpan Cheng, et al

Publication: ACS Catalysis

Publisher: American Chemical Society

Date: Dec 1, 2018

Copyright © 2018, American Chemical Society

PERMISSION/LICENSE IS GRANTED FOR YOUR ORDER AT NO CHARGE

This type of permission/license, instead of the standard Terms and Conditions, is sent to you because no fee is being charged for your order. Please note the following:

- Permission is granted for your request in both print and electronic formats, and translations.
- If figures and/or tables were requested, they may be adapted or used in part.
- Please print this page for your records and send a copy of it to your publisher/graduate school.
- Appropriate credit for the requested material should be given as follows: "Reprinted (adapted) with permission from {COMPLETE REFERENCE CITATION}. Copyright {YEAR} American Chemical Society." Insert appropriate information in place of the capitalized words.
- One-time permission is granted only for the use specified in your RightsLink request. No additional uses are granted (such as derivative works or other editions). For any uses, please submit a new request.

If credit is given to another source for the material you requested from RightsLink, permission must be obtained from that source.

BACK CLOSE WINDOW

Figure 19: Permission for the usage of image in figure 4 from American Chemical Society.

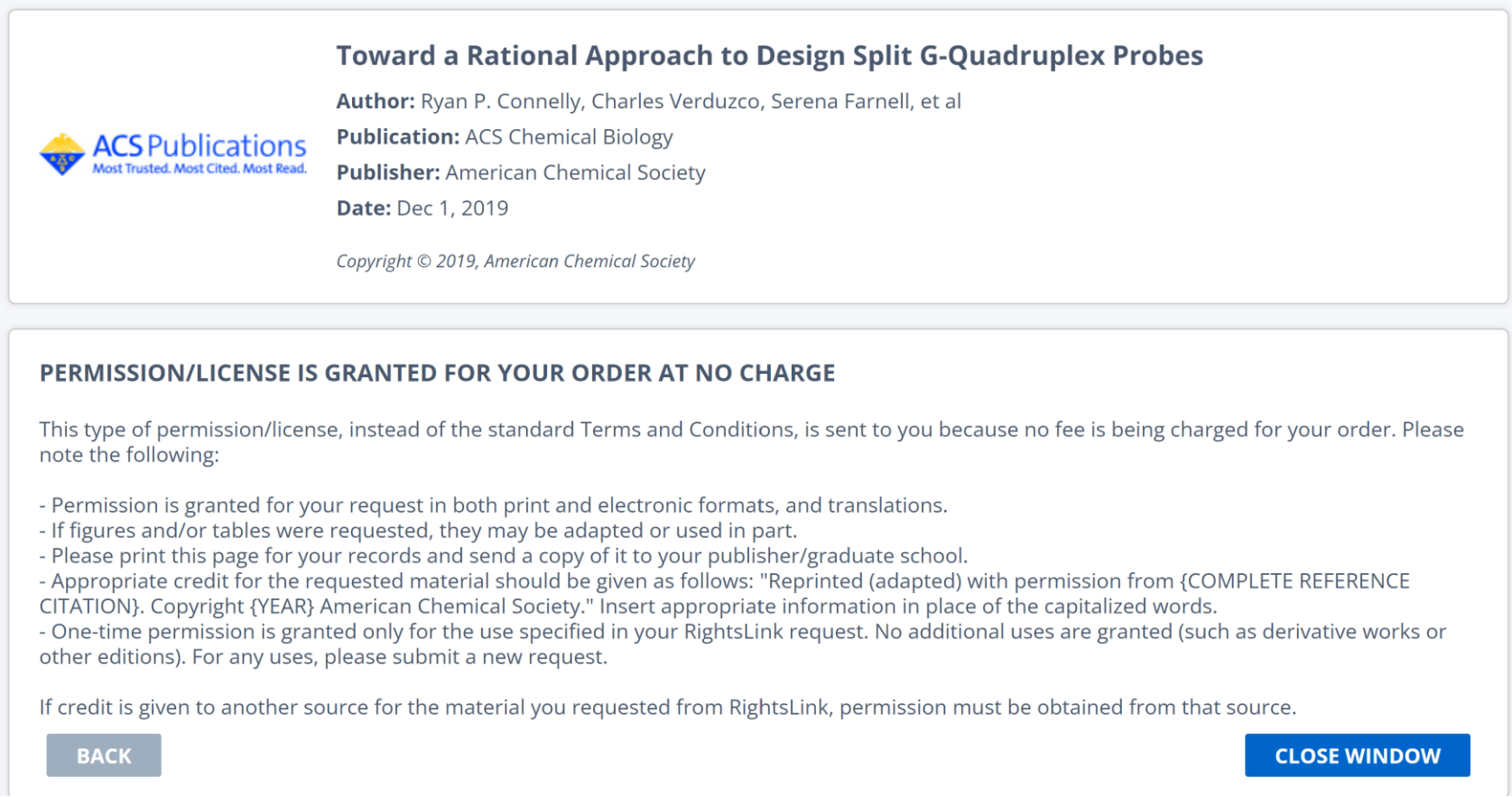

Toward a Rational Approach to Design Split G-Quadruplex Probes

Author: Ryan P. Connelly, Charles Verduzco, Serena Farnell, et al

Publication: ACS Chemical Biology

Publisher: American Chemical Society

Date: Dec 1, 2019

Copyright © 2019, American Chemical Society

PERMISSION/LICENSE IS GRANTED FOR YOUR ORDER AT NO CHARGE

This type of permission/license, instead of the standard Terms and Conditions, is sent to you because no fee is being charged for your order. Please note the following:

- Permission is granted for your request in both print and electronic formats, and translations.
- If figures and/or tables were requested, they may be adapted or used in part.
- Please print this page for your records and send a copy of it to your publisher/graduate school.
- Appropriate credit for the requested material should be given as follows: "Reprinted (adapted) with permission from {COMPLETE REFERENCE CITATION}. Copyright {YEAR} American Chemical Society." Insert appropriate information in place of the capitalized words.
- One-time permission is granted only for the use specified in your RightsLink request. No additional uses are granted (such as derivative works or other editions). For any uses, please submit a new request.

If credit is given to another source for the material you requested from RightsLink, permission must be obtained from that source.

BACK CLOSE WINDOW

Figure 20: Permission for the usage of image in figure 5 from American Chemical Society.

REFERENCES

[1] WHO Director-General's statement at the press conference following IHR Emergency Committee regarding the multi-country outbreak of Monkeypox - 23 July 2022. https://www.who.int/director-general/speeches/detail/who-director-general-s-statement-on-the-press-conference-following-IHR-emergency-committee-regarding-the-multi--country-outbreak-of-monkeypox--23-july-2022 (accessed Mar 19, 2023).

[2] Xiang, Y.; White, A. Monkeypox Virus Emerges from the Shadow of Its More Infamous Cousin: Family Biology Matters. *Emerging Microbes & Infections* **2022**, 11 (1), 1768–1777. DOI:10.1080/22221751.2022.2095309.

[3] Marennikova, S. S.; Šeluhina, E. M.; Mal'ceva, N. N.; Cimiskjan, K. L.; Macevic, G. R. Isolation and Properties of the Causal Agent of a New Variola-like Disease (Monkeypox) in Man. *Bulletin of the World Health Organization* **1972**, *46* (5), 599–611.

[4] Multi-country monkeypox outbreak in non-endemic countries. https://www.who.int/emergencies/disease-outbreak-news/item/2022-DON385 (accessed Mar 19, 2023).

[5] Alakunle, E. F.; Okeke, M. I. Monkeypox Virus: A Neglected Zoonotic Pathogen Spreads Globally. *Nature Reviews Microbiology* **2022**, *20* (9), 507–508. DOI:10.1038/s41579-022-00776-z.

[6] 2022 outbreak cases and data. https://www.cdc.gov/poxvirus/mpox/response/2022/index.html (accessed July 21, 2023).

[7] Mao, L.; Ying, J.; Selekon, B.; Gonofio, E.; Wang, X.; Nakoune, E.; Wong, G.; Berthet, N. Development and Characterization of Recombinase-Based Isothermal Amplification Assays (RPA/RAA) for the Rapid Detection of Monkeypox Virus. Viruses 2022, 14 (10), 2112. DOI:10.3390/v14102112.

[8] Drain, P. K.; Hyle, E. P.; Noubary, F.; Freedberg, K. A.; Wilson, D.; Bishai, W. R.; Rodriguez, W.; Bassett, I. V. Diagnostic Point-of-Care Tests in Resource-Limited Settings. *The Lancet Infectious Diseases* **2014**, *14* (3), 239–249. DOI:10.1016/s1473-3099(13)70250-0.

[9] Connelly, R. P.; Verduzco, C.; Farnell, S.; Yishay, T.; Gerasimova, Y. V. Toward a Rational Approach to Design Split G-Quadruplex Probes. ACS Chemical Biology 2019, 14 (12), 2701–2712. DOI:10.1021/acschembio.9b00634.

[10] Monkeypox: Experts give virus variants new names. https://www.who.int/news/item/12-08-2022-monkeypox--experts-give-virus-variants-new-names (accessed Dec 4, 2022).

[11] Mitjà, O.; Ogoina, D.; Titanji, B. K.; Galvan, C.; Muyembe, J.-J.; Marks, M.; Orkin, C. M. Monkeypox. *The Lancet* **2023**, 401 (10370), 60–74. DOI:10.1016/s0140-6736(22)02075-x.

[12] Breman, J. G.; Henderson, D. A. Diagnosis and Management of Smallpox. *New England Journal of Medicine* **2002**, 346 (17), 1300–1308. DOI:10.1056/nejmra020025.

[13] McCollum, A. M.; Damon, I. K. Human Monkeypox. *Clinical Infectious Diseases* **2013**, *58* (2), 260–267. DOI:10.1093/cid/cit703.

[14] Jezek, Z.; Szczeniowski, M.; Paluku, K. M.; Mutombo, M. Human Monkeypox: Clinical Features of 282 Patients. *Journal of Infectious Diseases* **1987**, *156* (2), 293–298. DOI:10.1093/infdis/156.2.293.

[15] Mbala, P. K.; Huggins, J. W.; Riu-Rovira, T.; Ahuka, S. M.; Mulembakani, P.; Rimoin, A. W.; Martin, J. W.; Muyembe, J.-J. T. Maternal and Fetal Outcomes among Pregnant Women with Human Monkeypox Infection in the Democratic Republic of Congo. *The Journal of Infectious Diseases* **2017**, *216* (7), 824–828. DOI:10.1093/infdis/jix260.

[16] Gul, I.; Liu, C.; Yuan, X.; Du, Z.; Zhai, S.; Lei, Z.; Chen, Q.; Raheem, M. A.; He, Q.; Hu, Q.; Xiao, C.; Haihui, Z.; Wang, R.; Han, S.; Du, K.; Yu, D.; Zhang, C. Y.; Qin, P. Current and Perspective Sensing Methods for Monkeypox Virus. *Bioengineering* **2022**, *9* (10), 571. DOI:10.3390/bioengineering9100571.

[17] Ma, A.; Langer, J.; Hanson, K. E.; Bradley, B. T. Characterization of the Cytopathic Effects of Monkeypox Virus Isolated from Clinical Specimens and Differentiation from Common Viral Exanthems. *Journal of Clinical Microbiology* **2022**, 60 (12). DOI:10.1128/jcm.01336-22.

[18] Monkeypox. https://www.who.int/news-room/fact-sheets/detail/monkeypox#:~:text=As%20orthopoxviruses%20are%20serologically%20cross,investigation%20where%20resources%20are%20limited. (accessed Mar 19, 2023).

[19] Peaper, D. R.; Landry, M. L. Laboratory Diagnosis of Viral Infection. *Neurovirology* **2014**, 123, 123–147. DOI:10.1016/b978-0-444-53488-0.00005-5.

[20] Adams, G. A Beginner's Guide to RT-PCR, qPCR and RT-qPCR. *The Biochemist* **2020**, *42* (3), 48–53. DOI:10.1042/bio20200034.

[21] Mészáros, É. QPCR: How SYBR® Green and Taqman® Real-Time PCR Assays Work. https://www.integra-biosciences.com/en/blog/article/qpcr-how-sybrr-green-and-taqmanr-real-time-pcr-assays-work (accessed 2023-07-25).

[22] Molecular Beacon Probes. https://www.idtdna.com/pages/products/qpcr-and-pcr/custom-probes/molecular-beacons (accessed 2023-07-25).

[23] Yang, C. J.; Tan, W.; Wang, C. In Molecular Beacons; *Springer*, **2013**; pp 45–54.

[24] Li, Y.; Zhao, H.; Wilkins, K.; Hughes, C.; Damon, I. K. Real-Time PCR Assays for the Specific Detection of Monkeypox Virus West African and Congo Basin Strain DNA. *Journal of Virological Methods* **2010**, 169 (1), 223–227. DOI:10.1016/j.jviromet.2010.07.012.

[25] *Test Procedure: Monkeypox virus Generic Real-Time PCR Test*. Centers for Disease Control & Prevention. 2022. https://www.cdc.gov/poxvirus/mpox/pdf/PCR-Diagnostic-Protocol-508.pdf (accessed 2023-07-25).

[26] Kolpashchikov, D. M. Binary Probes for Nucleic Acid Analysis. *Chemical Reviews* **2010**, *110* (8), 4709–4723. DOI:10.1021/cr900323b.

[27] Stancescu, M.; Fedotova, T. A.; Hooyberghs, J.; Balaeff, A.; Kolpashchikov, D. M. Nonequilibrium Hybridization Enables Discrimination of a Point Mutation within 5–40 °C. Journal of the American Chemical Society 2016, 138 (41), 13465–13468. DOI:10.1021/jacs.6b05628.

[28] Kolpashchikov, D. M. Split DNA Enzyme for Visual Single Nucleotide Polymorphism Typing. *Journal of the American Chemical Society* **2008**, *130* (10), 2934–2935. DOI:10.1021/ja711192e.

[29] Yang, H.; Zhou, Y.; Liu, J. G-Quadruplex DNA for Construction of Biosensors. *TrAC Trends in Analytical Chemistry* **2020**, 132, 116060. DOI:10.1016/j.trac.2020.116060.

[30] Capra, J. A.; Paeschke, K.; Singh, M.; Zakian, V. A. G-Quadruplex DNA Sequences Are Evolutionarily Conserved and Associated with Distinct Genomic Features in Saccharomyces Cerevisiae. *PLoS Computational Biology* **2010**, 6 (7). DOI:10.1371/journal.pcbi.1000861.

[31] Chen, J.; Zhang, Y.; Cheng, M.; Guo, Y.; Šponer, J.; Monchaud, D.; Mergny, J.-L.; Ju, H.; Zhou, J. How Proximal Nucleobases Regulate the Catalytic Activity of G-Quadruplex/Hemin DNAzymes. *ACS Catalysis* **2018**, *8* (12), 11352–11361. DOI:10.1021/acscatal.8b03811.

[32] Qiu, D.; Mo, J.; Liu, Y.; Zhang, J.; Cheng, Y.; Zhang, X. Effect of Distance from Catalytic Synergy Group to Iron Porphyrin Center on Activity of G-Quadruplex/Hemin DNAzyme. *Molecules* **2020**, *25* (15), 3425. DOI:10.3390/molecules25153425.

[33] Chen, J.; Guo, Y.; Zhou, J.; Ju, H. The Effect of Adenine Repeats on G-Quadruplex/Hemin Peroxidase Mimicking DNAzyme Activity. *Chemistry - A European Journal* **2017**, *23* (17), 4210–4215. DOI:10.1002/chem.201700040.

[34] Chang, T.; Gong, H.; Ding, P.; Liu, X.; Li, W.; Bing, T.; Cao, Z.; Shangguan, D. Activity Enhancement of G-Quadruplex/Hemin DNAzyme by Flanking d(CCC). *Chemistry - A European Journal* **2016**, *22* (12), 4015–4021. DOI:10.1002/chem.201504797.

[35] Li, W.; Li, Y.; Liu, Z.; Lin, B.; Yi, H.; Xu, F.; Nie, Z.; Yao, S. Insight into G-Quadruplex-Hemin DNAzyme/RNAzyme: Adjacent Adenine as the Intramolecular Species for Remarkable Enhancement of Enzymatic Activity. *Nucleic Acids Research* **2016**, *44* (15), 7373–7384. DOI:10.1093/nar/gkw634.

[36] Deng, M.; Zhang, D.; Zhou, Y.; Zhou, X. Highly Effective Colorimetric and Visual Detection of Nucleic Acids Using an Asymmetrically Split Peroxidase DNAzyme. *Journal of the American Chemical Society* **2008**, *130* (39), 13095–13102. DOI:10.1021/ja803507d.

[37] Zhu, J.; Zhang, L.; Dong, S.; Wang, E. How to Split a G-Quadruplex for DNA Detection: New Insight into the Formation of DNA Split G-Quadruplex. *Chemical Science* **2015**, *6* (8), 4822–4827. DOI:10.1039/c5sc01287b.

[38] Santoro, S. W.; Joyce, G. F. A General Purpose RNA-Cleaving DNA Enzyme. Proceedings of the National Academy of Sciences 1997, 94 (9), 4262–4266. DOI:10.1073/pnas.94.9.4262.

[39] Mokany, E.; Bone, S. M.; Young, P. E.; Doan, T. B.; Todd, A. V. MNAzymes, a Versatile New Class of Nucleic Acid Enzymes That Can Function as Biosensors and Molecular

Switches. *Journal of the American Chemical Society* **2010**, *132* (3), 1051–1059. DOI:10.1021/ja9076777.

[40] Gerasimova, Y. V.; Cornett, E. M.; Edwards, E.; Su, X.; Rohde, K. H.; Kolpashchikov, D. M. Deoxyribozyme Cascade for Visual Detection of Bacterial RNA. *ChemBioChem* **2013**, *14* (16), 2087–2090. DOI:10.1002/cbic.201300471.

[41] Dhar, B. C.; Reed, A. J.; Mitra, S.; Rodriguez Sanchez, P.; Nedorezova, D. D.; Connelly, R. P.; Rohde, K. H.; Gerasimova, Y. V. Cascade of Deoxyribozymes for the Colorimetric Analysis of Drug Resistance in Mycobacterium Tuberculosis. *Biosensors and Bioelectronics* **2020**, *165*, 112385. DOI:10.1016/j.bios.2020.112385.

[42] Zadeh, J. N.; Steenberg, C. D.; Bois, J. S.; Wolfe, B. R.; Pierce, M. B.; Khan, A. R.; Dirks, R. M.; Pierce, N. A. NUPACK: Analysis and Design of Nucleic Acid Systems. *Journal of Computational Chemistry* **2011**, *32* (1), 170–173. DOI:10.1002/jcc.21596.

[43] Pierce, K. E.; Sanchez, J. A.; Rice, J. E.; Wangh, L. J. Linear-after-the-Exponential (Late)-PCR: Primer Design Criteria for High Yields of Specific Single-Stranded DNA and Improved Real-Time Detection. *Proceedings of the National Academy of Sciences* **2005**, *102* (24), 8609–8614. DOI:10.1073/pnas.0501946102.

[44] Reed, A. J.; Connelly, R. P.; Williams, A.; Tran, M.; Shim, B.-S.; Choe, H.; Gerasimova, Y. V. Label-Free Pathogen Detection by a Deoxyribozyme Cascade with Visual Signal Readout. *Sensors and Actuators B: Chemical* **2019**, 282, 945–951. DOI:10.1016/j.snb.2018.11.147.

[45] Ida, J.; Kuzuya, A.; Choong, Y. S.; Lim, T. S. An Intermolecular-Split G-Quadruplex DNAzyme Sensor for Dengue Virus Detection. *RSC Advances* **2020**, *10* (55), 33040–33051. DOI:10.1039/d0ra05439a.

[46] Suñer, C.; Ubals, M.; Tarín-Vicente, E. J.; Mendoza, A.; Alemany, A.; Hernández-Rodríguez, Á.; Casañ, C.; Descalzo, V.; Ouchi, D.; Marc, A.; Rivero, À.; Coll, P.; Oller, X.; Miguel Cabrera, J.; Vall-Mayans, M.; Dolores Folgueira, M.; Ángeles Melendez, M.; Agud-Dios, M.; Gil-Cruz, E.; Paris de Leon, A.; Ramírez Marinero, A.; Buhiichyk, V.; Galván-Casas, C.; Paredes, R.; Prat, N.; Sala Farre, M.-R.; Bonet-Simó, J. M.; Farré, M.; Ortiz-Romero, P. L.; Clotet, B.; García-Patos, V.; Casabona, J.; Guedj, J.; Cardona, P.-J.; Blanco, I.; Marks, M.; Mitjà, O.; Ramón Santos, J.; Bailón, L.; Benet, S.; Arroyo Andres, J.; Calderón Lozano, L.; Carrasco Díaz, M.; Budria Serrano, C.; Crespillo Galán, E.; Parra Manzano, A. I.; Nef Rabadán, P.; Muntané, L.; Sánchez-Lafuente Doncel, C.; Marrero Pueo, Y. M.; Muñoz Quinto, A.; Acosta, M.; Alvarez, P.; Arando, M.; García, J. N.; Monforte, A.; Maltas Hidalgo, Y.; Hervas Perez, R.; Clotet Romero, L. Viral Dynamics in Patients with Monkeypox Infection: A Prospective Cohort Study in Spain. *The Lancet Infectious Diseases* **2023**, *23* (4), 445–453. DOI:10.1016/s1473-3099(22)00794-0.